CHALMERS
UNIVERSITY OF TECHNOLOGY

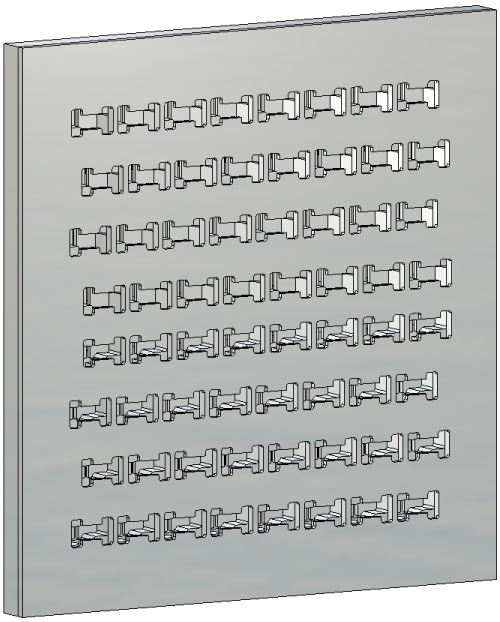

Phased array antenna with series fed transverse slots Based on Gap-waveguide Technology

Master's thesis in Wireless, Photonics and Space Engineering

Julius Petersson

Department of Electrical Engineering
CHALMERS UNIVERSITY OF TECHNOLOGY
Gothenburg, Sweden 2020

Master's thesis 2018:NN

Phased array antenna with series fed transverse slots Based on Gap-waveguide Technology

Julius Petersson

CHALMERS
UNIVERSITY OF TECHNOLOGY

Department of Electrical Engineering
Antenna group
Chalmers University of Technology
Gothenburg, Sweden 2018

1D H-plane Beam Steering Antenna
Based on Gap-waveguide Technology
JULIUS PETERSSON

© JULIUS PETERSSON, 2020.

Supervisor: Assistant Professor Ashraf Uz Zaman
Examiner: Professor Jian Yang

Master's Thesis 2018:NN
Department of Electrical Engineering
Antenna group
Chalmers University of Technology
SE-412 96 Gothenburg
Telephone +46 31 772 1000

Cover: Render of final array design

Typeset in LaTeX
Gothenburg, Sweden 2018

Phased array antenna with series fed transverse slots Based on Gap-waveguide Technology

JULIUS PETERSSON
Department of Electrical Engineering
Chalmers University of Technology

Abstract

This thesis presents the design of a 1D beam steering antenna based on Gap-waveguide Technology for use as a base station antenna in next generation wireless telephone systems. The gap waveguide is a developing technology based on an artificial magnetic conductor structure of periodic pins which enables contact-less electromagnetic isolation. The technology is aimed to solve the issues with contemporary technologies and be a base to develop highly efficient and inexpensive antennas for millimeter wave frequencies.

The antenna is designed to provide orthogonal polarization to traditional slot waveguide antennas while keeping compatability with existing designs for element feeding. The final design achieves an impedance bandwidth of 7% with acceptable radiation patterns but show promise for future optimization.

Keywords: gap waveguides, slot array antenna, transverse slots, AMC, double-corner-cut square waveguide.

Contents

List of Figures

List of Tables

1

Introduction

1.1 Background

A new generation of mobile communication technology is currently in development by the telecommunication industry. This fifth generation standard (5G) promises to deliver a hundredfold increase in network capacity. This major increase of required bandwidth has led engineers to look to mmWave frequencies for available spectrum far above the traditional frequency bands. At these frequencies new opportunities as well as drawbacks with conventional waveguide technologies arise. The increased path-losses as well as inefficiencies in amplification create a need for low-cost, low-loss solutions for antennas. Technologies presently used like microstrip lines and hollow waveguides exhibit a number of issues at these frequencies such as high dielectric losses as well as challenges with manufacturing and integration with electronics. The gap waveguide is a developing technology based on an artificial magnetic conductor structure of periodic pins which enables contact-less electromagnetic isolation. The technology is aimed to solve the increasingly limiting issues with the implementation of traditional waveguide structures at millimetre wave frequencies (30 GHz) and above. [1]

	Hollow waveguides	Microstrip	SIW	Gap waveguides
Losses	Low	High	High	Low
Cost	High	Low	Medium	Low

Table 1.1: Pros and cons of different waveguide technologies

Compared to conventional hollow waveguides, the Gap waveguide technology has lower requirements on precision manufacturing and assembly procedures which has mostly limited hollow waveguides implementations due to high costs. The Gap waveguide technology keeps the low-loss characteristics of the hollow waveguide while mitigating some of the drawbacks in manufacturing.[2]

Compared to planar, low to medium cost and substrate based waveguides such as microstrip line, co-planar waveguides (CPW) or surface integrated waveguides (SIW) the Gap waveguide technology avoids the high losses due to propagation through a lossy dielectric medium. These losses can be up to tens of dB per meter for substrate based waveguides, compared to a fraction of a dB for hollow and gap waveguides.[2]

Gapwaves AB is a start-up founded by late Per-Simon Kildal with a large patent portfolio in gap-waveguide technology. Gapwaves specialize in antennas for next generation telecommunications and automotive applications and is headquartered in Gothenburg, Sweden.

1.2 Aim

The goal of the thesis is to design, manufacture and test a 1D beam steering antenna based with gap waveguide technology. The intended use case will be in a mmWave 5G base station module for high bandwidth communication. The target frequency is 28 GHz, based on the frequency bands used for 5G trails in the U.S. covering a fractional bandwidth of 13%. [3]

Current PCB-based designs are characterized with high ohmic losses, in [4] an 8 x 8 patch antenna array is presented for 5G applications, due to the nature of propagation through a dielectric substrate at mmWave-frequencies the antenna with feeding presents a loss of more than 6 dB, effectively reducing the radiated power with 75%. Similar losses for a gap waveguide based solution would be in the ranges of 1.5 dB, including filters and PCB-to-waveguide transitions [3].

The high capacity that 5G promises to deliver requires the efficient use of the allocated electromagnetic spectrum, because of this the base stations under development will make use of both polarization and spatial diversity. The spatial diversity will be implemented with 1D beam steering, allowing the base station to dynamically direct the transmitted and received power to the terminal with a linear phase offset on the antenna elements. The beam steering should allow for scanning 45 degrees to each side in the horizontal plane and 10 degrees up and down, which sets limitations on the element spacing in both azimuth and elevation. This azimuth scan would allow two base station modules in pair cover a 90 degree field of view, suitable for placement on the side of a building, or four antennas for a full 360 degree field of view.[3]

Low loss sub-arrays are used to increase the gain by reducing the beam width in elevation, trading coverage in elevation for increased EIRP (Equivalent Isotropic Radiated Power), this is possible due to the limited range of movement in elevation for terminals in a cell based network.[3] The polarization diversity will be provided with a modular design allowing the assembly of a pair of antennas with orthogonal polarization while keeping filter and beam steering electronics completely interchangeable.[5]

As a final product, the array would most likely be scaled up to 16 x 16 elements for an ever higher EIRP, but 8 x 8 elements are considered enough for prototyping for which results can be extrapolated to the larger aperture.

1.3 Limitations

The thesis will not cover the filters nor the beam steering electronics that will be part of the complete and integrated antenna module. To facilitate testing on the antenna layer, the antenna will be fed with waveguide launchers on a PCB with coaxial connectors to interface with the measurement equipment.

2

Gap Waveguides

The gap waveguide is a novel technology aimed to solve the increasingly limiting issues with the implementation of traditional waveguide structures at millimetre wave frequencies (30 GHz) and above. Conventional hollow waveguides require precision manufacturing and assembly procedures which limits the potential usage of the technology for non-military electronics due to high costs while planar, low cost and substrate based waveguides such as microstrip line, co-planar waveguides (CPW) or surface integrated waveguides (SIW) introduces high losses due to the wave propagation through a lossy dielectric medium. The gap waveguide provides low loss propagation combined with ease of manufacturing, allowing the use of air filled waveguide structures in high-volume low-cost millimetre wave applications such as telecommunication and automotive.[2]

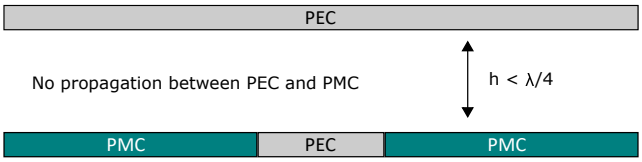

Figure 2.1: Ideal model of gap waveguide

In the ideal case, the gap waveguide is a parallel plate waveguide with a perfect electric conductor (PEC) on top and a PEC bordered on both sides with a perfect magnetic conductor (PMC) on the bottom. As long as the distance between the plates is less than $\lambda/4$ no wave propagation will be possible between the PEC and PMC and the energy is confined in the center between the two PEC, illustrated in Fig. 2.1.[1]

While a PEC can be approximated with a metal such as aluminum or brass, there is, unfortunately, no substitute to a PMC in real life. For this, the gap waveguide technology introduces a pin-based artificial magnetic conductor (AMC) meta material, which unit cell is shown in Fig. 2.3. The AMC creates a virtual wall on both sides of the waveguide section over its effective frequency range preventing the electric field from leaking out the sides without the need of perfect galvanic contact between the top and bottom plates as in a traditional hollow waveguide.[1]

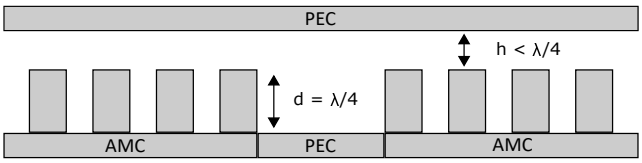

Figure 2.2: Groove gap waveguide

The pin-based AMC creates an electromagnetic band-gap (EBG) structure, which splits the cut-off frequencies between the first and second order modes, creating a band gap where electromagnetic propagation is not possible.[2]

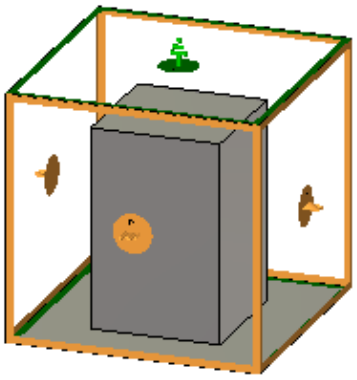

Figure 2.3: AMC Unit Cell

The bandgap can be analyzed over the Brillouin zone seen in Fig. 2.3 with the Eigenmode solver in CST. The dispersion diagram for a infinite pin structure with a pin height of 2.1 mm, a pin width of 1.35 mm, a period of 2.65 mm and a gap height of 0.25 mm can be seen in Fig 2.4. The simulations show the band gap that occurs between mode 1 and 2, effectively stopping any

propagation through the unit cell between 23.75 GHz and 56.5 GHz. The band gap is the region for which the gap waveguides work equivalent to the ideal case. The size of the pins need to be chosen to ensure that this region covers the bandwidth of the design.[2]

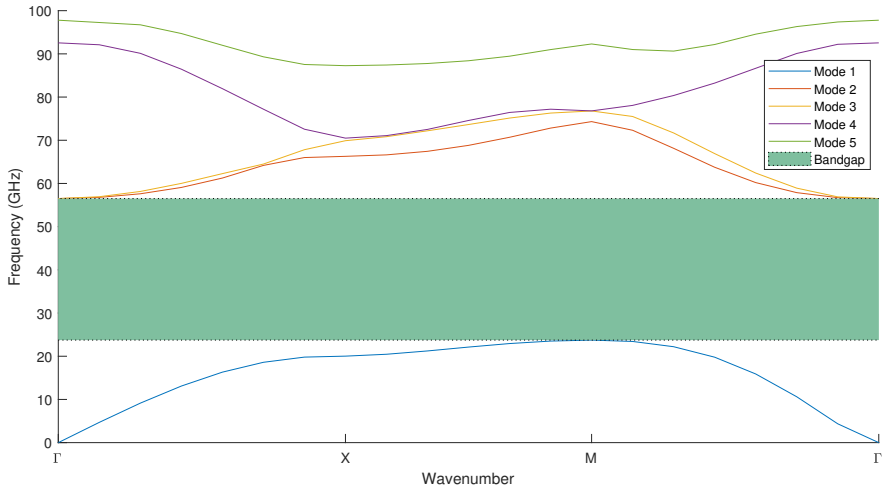

Figure 2.4: Dispersion diagram

Many traditional waveguide structures have corresponding equivalent gap waveguide structures. Three major guiding structures can be found described in literature: the groove, ridge and inverted microstrip gap waveguides. The similarity between the gap waveguides and the hollow waveguides means that established literature and conventions for hollow waveguides can be applied to the gap waveguide platform with only small adjustments.[1]

The groove gap waveguide, seen in Fig. 2.2 has a field distribution very similar to the normal rectangular hollow waveguide's TE_{10} and is the most basic of the gap waveguides. It is simple to design and manufacture, but takes up comparatively much space.[2]

The ridge gap waveguide is a gap waveguide with a large capacitive load in the form of a ridge in the center, providing a quasi-TEM mode between the ridge and the top plate. The main benefit of the ridge waveguide is that the ridge increases the cut-off space between the dominant and second order modes [6], allowing a waveguide of identical outer dimensions to be used over

a larger bandwidth. Due to the shift in frequency of the cut-off frequency of the fundamental mode, the width and height of the ridge waveguide can be decreased while still allowing the wave propagation of the fundamental mode. The dimensions of the ridge can be used to control the guided wavelength of the propagating wave. These parameters can be used to fulfill the criteria set by Eq. (3.7).

Around these guiding structures it is possible to apply traditional design techniques to create easily manufacturable and high performance distribution networks resonant filters and slot antennas, as well as transitions between the gap waveguide structures and PCB-based waveguides such as microstrip line.[1]

2.1 Gap waveguide designs

The gap waveguide technology has successfully been used to realize passive microwave designs over a large range of frequencies and applications. These designs validate the gap waveguide technology as an emerging platform for mmWave-frequency applications.

2.1.1 76 GHz Automotive radar

In [7], a center-fed slotted waveguide antenna for automotive bi-static radar applications at E-band is presented. The antenna column provides excellent realized gain with very low losses in an design well suited for mass production at high volumes. The antenna is designed for use in driver assistance systems where the high dielectric losses in current microstrip designs degrade the performance of the radar due to a lower signal-to-noise ratio. The slotted waveguide antenna is implemented as a resonant slotted waveguide, with a virtual short circuit at the end of the feeding waveguide with a width of half a wavelength.

2.1.2 Fixed beam antennas

In [8] the gap-waveguide technology is used to fulfill the ETSI Class II Radiation pattern with a corporate fed gap-waveguide array antenna for V-band with high realized gain. The intended application is multi-Gbps point-to-point communication links. The antenna is built up in three layers without the need of electrical contact due to the gap-waveguide technology. The impedance bandwidth is 17.6% with a reflection coefficient better than $-10\,\mathrm{dB}$. The antenna is designed as a 2 x 2 cavity-backed sub-array which is then combined into a 16 x 16 slot array to provide a directive beam, due to this design choice, the antenna can be scaled for multiple configurations depending on the application.

In [9] a 16 x 16 slot flat panel array antenna with a monopulse comparator

feeding network at W-band is presented. This design includes a gap waveguide magic tee in order to realize the comparator feeding network compact and low-profile. The network allows a monopulse radar to track an object with a single transmitted pulse by providing four feeds with different combinations of sums and differences of the received echo for each 8 x 8 quadrant sub-array.

In [10] an 8 x 8 dual polarized flat panel array antenna with a circular radiating element is presented. The two orthogonal polarizations have separate feeds in order to make use of polarization diversity for increased throughput, especially used in satellite communication applications.

In [11] an 8 x 8 slot 60 GHz flat panel antenna is presented, this design implements the the corporate feed network as a single layer resulting in a very thin final design.

2.1.3 Beam scanning antennas

In [12] a complete beam steering antenna module with active analog phase shifters, transitions from PCB to low loss gap waveguides, filters, and a high gain slot array antenna elements is presented. The module is designed for base station use cases for 5G mmWave telecommunication and shows the great versatility of the gap waveguide technology as we approach the increased use of mmWave-frequency bands. Low losses in feeding is of essence to compensate for the high propagation losses at the design frequencies and the integration of high-Q filters prevent the leakage into neighbouring frequency bands occupied by sensitive satellite communication.

The gap waveguide technology has also been shown in applications integrated with substrate based elements, in [13] a corporate fed wide-band patch antenna array is presented. In this design, the routing is implemented with ridge gap waveguides, which excite substrate based patch antenna elements coupled through a slot. The advantage compared to [8] is that the cavity layer and the slot layer can be combined to a single substrate, while still keeping the routing in the low loss gap waveguide technology.

2.1.4 Integration with active components

One drawback with the gap waveguide technology, as with hollow waveguides in general, is the interface towards integrated circuits such as MMICs which are designed to be placed on top of a PCB. This requires the design of good performing transitions between microstrip lines and gap waveguides. In [14], a compact, low-loss, microstrip to ridge gap waveguide transition is presented. The transition relies on the similarities between the QTEM-modes between the two waveguide technologies, this means that the field can be transformed by tapering the ridge width from the narrower microstrip to a wider ridge gap waveguide with a standard Chebychev transformer. A drawback with this design is that it requires electrical contact between the microstrip-line and the ridge. In [15] a transition without this requirement is presented.

In [16] another planar transition between microstrip and groove gap waveguide at W-band is presented. The resonator probe is similar to that in [15] but this transition does not require a back-short under the probe, which allows for a very compact design. Another transition can be found in [17], here the microstrip probe couples to a full size rectangular waveguide straight above the cavity, moving from a horizontal to vertical propagation.

With the growing interest of hollow and gap waveguide based antennas for telecom and automotive a point might come in the future where the IC interface directly with the waveguide, removing the need of high-cost/high-performance RF-PCBs and bond-wires to further reduce losses and manufacturing complexities. One such MMIC-to-waveguide transition is presented in [18].

3

Slotted waveguide array antennas

3.1 Polarization

Electromagnetic waves can be described as transverse waves and thus has an oscillation that is oriented perpendicular to the wave propagation called the wave's polarization. Polarization is a fundamental concept in antenna engineering and antennas are generally designed with a single linear (vertical/horizontal or $\pm 45°$) polarization or with a circular polarization (right- / left-hand). The polarization is defined with regards to the E-field component of the electromagnetic wave and can be described as the combination of two components, the desired co-polarization (E_{co}) and the undesired cross-polarization (E_{xp}) which are parallel to the unit vectors $\hat{\mathbf{co}}$ and $\hat{\mathbf{xp}}$ respectively which gives us the following expression for the e-field

$$\mathbf{E} = \left(E_{co}\hat{\mathbf{co}} + E_{xp}\hat{\mathbf{xp}}\right) e^{-jk_0 z} \tag{3.1}$$

The ratio between the magnitudes of the co- and cross-polarization components is called the polarization isolation or decoupling

$$(\mathrm{XPD})_{\mathrm{dB}} = 10\log|E_{co}/E_{xp}|^2\mathrm{dB} \tag{3.2}$$

which is a crucial parameter in some application as it enables the discrimination of waves of different polarizations by aligning the transmitting and receiving antennas correctly. This allows systems to reuse frequencies to essentially send twice as much data in the same space, a technique called polarization diveristy.[5]

3.1.1 Polarization in multipath environments

A multipath environment introduces selective polarization fading as the wave propagates and reflects in a statistically random fashion. This, combined with the fact that the orientation of a handset is unknown to a mobile network base station creates an imperative to transmit and receive the two orthogonal polarizations.[5]

3.1.2 Phased array antenna

An antenna array is a combination of multiple antenna elements working together as a single antenna. The directivity of a single element antenna without reflectors is low which is less suitable for high throughput communication. To increase the gain, the energy from the transmitter is split into multiple antenna elements which radiation patterns interfere constructively and destructively to increase the radiated power in the desired direction while decreasing the radiated power in others shown in Fig.3.1 . Due to the fundamental property of reciprocity this interference works the same for receiving antennas.[5]

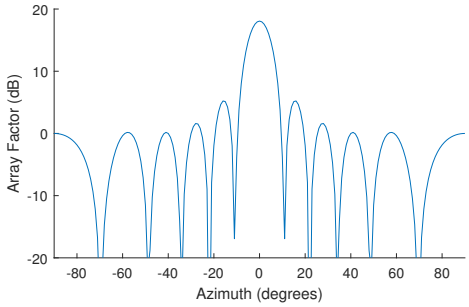

Figure 3.1: Array factor for 8-element uniform linear array with $d = 2/3\lambda$

The resulting radiation pattern can be obtained by multiplying the radiation pattern of the individual element with the array factor (AF). The array factor is a function of the magnitude (I) and relative phase difference of each element (β) as well as the element spacing (d) for both dimensions and is calculated as follows

$$AF = S_{xm} S_{yn} \tag{3.3}$$

$$S_{xm} = \sum_{m=1}^{M} I_{m1} e^{j(m-1)(kd_x \sin\theta \cos\phi + \beta_x)} \tag{3.4}$$

$$S_{ny} = \sum_{n=1}^{N} I_{1n} e^{j(n-1)(kd_y \sin\theta \sin\phi + \beta_y)} \tag{3.5}$$

$$D_{array}(\theta, \varphi) = AF * D_{element}(\theta, \varphi) \tag{3.6}$$

The dependence on the amplitude and phase of the element excitations presents both challenges and opportunities in the design of antenna arrays. The standard form, with an element spacing of λ and uniform amplitude distribution results in maximum possible directivity with a side lobe level of $-13.2\,\mathrm{dB}$ while an amplitude taper, where the amplitude is lower in the outer elements of the array, leads to lower side lobe levels (SLL) at the cost of directivity. A linear phase distribution of the element excitation can be used to steer the main beam along the axes of the array, while a non-linear phase distribution leads to lower directivity.[5]

The relative phase difference of each slot can be used to steer the main beam in a desired direction by creating a equal phase front in that direction, shown in Fig. 3.2a. The maximum steering angle is a function of the wavelength and inter element spacing. If the spacing is too wide multiple equal phase fronts emerge and the directivity is split in multiple directions called grating lobes shown in 3.2b. This occurs when the distance between each element is larger than

$$d_{max} = \frac{\lambda}{1 + \sin\theta_{steer,max}} \tag{3.7}$$

where $\theta_{steer,max}$ is the maximum required scanning angle.

The relative phase difference between two adjacent elements for a specific main beam angle (θ_{steer}) is calculated as

$$\beta = \frac{360° d \sin\theta_{steer}}{\lambda} \tag{3.8}$$

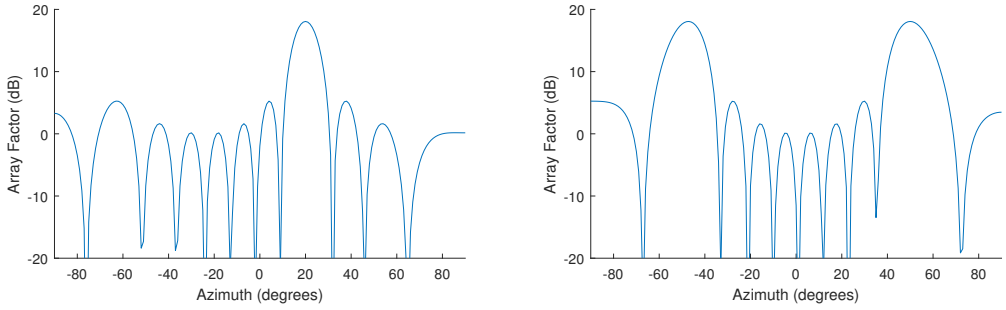

(a) $\beta = 82°$ for $\theta_{steer} = 20°$ **(b)** $\beta = 183°$ for $\theta_{steer} = 50°$

Figure 3.2: Array factor for 8-element uniform linear array with $d = 2/3\lambda$ for different θ_{steer}

3.2 Slotted waveguide antenna

Slotted waveguide antennas have been used in microwave electronics since the 1950:ies and have proved itself to be an efficient, easy to manufacture and design, and durable way to feed antenna elements in a linear array.[5]

The array is created by opening up slots blocking the surface currents on the waveguide wall. The displacement of the surface currents create a voltage over the slot which allows the slot to radiate. [5]

Multiple configurations of slots are possible by varying the position and rotation of the slots to control the phase, magnitude and polarization of the

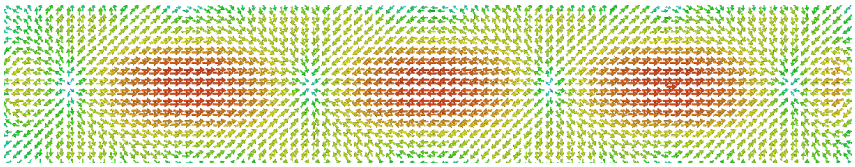

Figure 3.3: Surface current on top of rectangular waveguide

radiated field. These variables must be carefully chosen based on the design objectives to achieve the demanded far field distribution. [5]

3.2.1 Longitudinal slots

The classical way to reduce the slot spacing of radiating slots on the broad side of a rectangular waveguide is to place them in the longitudinal direction along the length of the waveguide.[5]

The longitudinal slots are excited by restricting the flow of the transverse surface current on the waveguide, which is largest at either side of the current minima. The longitudinal orientation exploits the fact that the transverse current is of opposite direction on the two sides of the center of the rectangular waveguide. Because of this, the slots can be placed at an element spacing of $\lambda_g/2$ but still radiate in phase when placed alternating on the left and right side. As the slot is excited by transverse current, the longitudinal slots radiate with a polarization orthogonal to length of the waveguide.[5]

3.2.2 Transverse slots

To achieve the orthogonal polarization to the longitudinal slot, i.e. a polarization along the waveguide length, with a slot on the broad wall of the waveguide one must rotate the slots 90 degrees. The maximum surface currents are located along the center of the waveguide. However, the longitudinal surface currents lack the same anti-symmetry as the transverse currents do, which removes any possibility to excite array elements in phase except in whole λ_g intervals which results in grating lobes.[19]

Two possible solutions to the grating lobe issue is found in literature. The first solution is to lower λ_g by introducing a dielectric load inside the waveguide. However, this is not desirable as the losses are too high at the frequencies of interest.

The second solution found in [20] is to introduce baffles in the evanescent region of the far field to suppress the grating lobes, but the placement of the elements differs from those in the longitudinal case which makes it difficult to implement the transverse slots on an identical feeding network.

3.2.3 Twist / Cavity

Yet another alternative is to keep the longitudinal slots on top of the waveguide and rotate the polarization afterwards. Reusing the longitudinal slots is preferable as it allows the reuse of the feeding waveguide for both polarizations without any modifications which reduces manufacturing complexity. Unfortunately, the literature behind such solution is lacking for linear polarization but has been successfully used in [21] and [22] to create circularly polarized antennas with series fed slots.

3.2.4 Slot array topology

The feeding waveguide can either be terminated with a matched load, creating a travelling wave slot array antenna, or a short circuit, creating a resonant wave slot array antenna.

The travelling wave slot array antenna has energy entering from one end, propagating along the waveguide to excite the slots to finally have the remaining energy absorbed in the load. The travelling wave slot array requires that each slot radiates a fraction of the incoming energy and lets most energy travel on while keeping the reflected power from sending energy back in the opposite direction. Traveling wave slot arrays can be made very long with a wideband impedance match at the port but have issues with squinting of the main beam with varying frequency.

The standing wave slot array antenna instead supports a standing wave pattern due to the superposition of the incident wave and the reflected wave from the shorted load. The standing wave pattern at the center frequency is used to position the slots for desired amplitude and phase distribution.

3.3 Waveguide twist

A waveguide twist is a gradual or discrete rotation of the waveguide structure in order to orient the electromagnetic field in a microwave system. The twists can be used both to route the waveguide to solve geometric problems as well as provide functional arrangement of microwave systems. Rotations of 90 degrees are used to connect components between two orthogonal polarizations and 180 degree rotations are used to invert the phase of a transmitted wave. Research has been done to create wideband compact solutions to the waveguide twist.

The traditional way is to twist the rectangular wave guide tube continuously. They provide excellent bandwidth but are not suitable for integrated systems manufactured from metal blocks due to their non-discrete steps. The drawback of the continuous twist is that they are long and not easy to integrate in a milled or casted structure due to tool obstruction and insufficient draft. The last part can be solved by rotating the waveguide with multiple, slightly rotated, wave guide sections as shown in [23].

3.3.1 Double-corner-cut twist

A waveguide twist can also be created by introducing cross coupling between the two orthogonal polarizations in a square waveguide. This can be achieved by introducing an asymmetry at a 45° angle.

The double corner-cut waveguide is a square waveguide with two cut corners on the diagonal line to facilitate the coupling between the horizontal and vertical polarizations. It has been shown to work as a two step polarization twister over a 30% bandwidth at the -30 dB level in [24] at a length of less

than a quarter λ_g.

Without the cuts, the square waveguide has two dominant modes TE_{10} and TE_{01} which are uncoupled to each other. Introducing the cuts couples the two dominant modes and split their resonant frequencies. The dominant mode (TE_{1e}) has its electric field concentrated between the two cuts oriented at a 45° angle similar to a dual ridge waveguide and the second order mode's (TE_{1m}) is orthogonal to the first mode. The modes can be seen as a pertubed difference and sum combination between the TE_{10} and TE_{01} modes of the square waveguide.

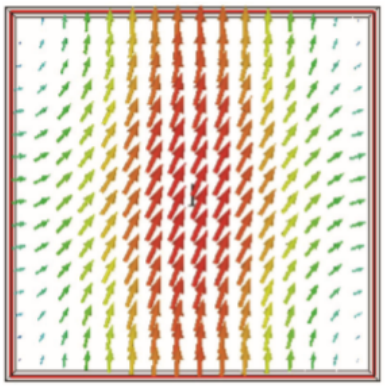

Figure 3.4: Square waveguide E-field pattern

The cutoff frequency of the double corner-cut waveguide is dependent on the width (a) and cut (s). The dominant mode TE_{1m} has a normalized cutoff wavelength going from $a/\lambda_{cut} = 0.5$ when $s/a = 0$ corresponding to a square waveguide with the side $a = 0.5\lambda_{cut}$ to $a/\lambda_{cut} = 0.0$ when $s/a = 0.5$ essentially closing the gap and creating two separate waveguides[24].

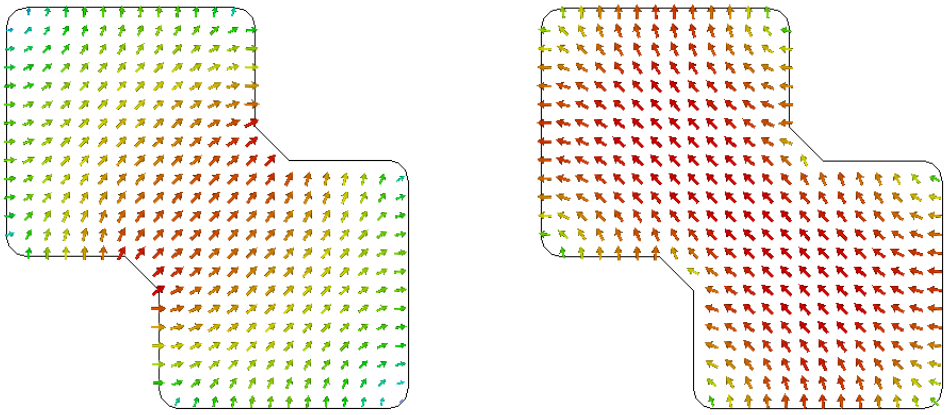

(a) Dominant mode (TE_{1e}) **(b)** Second order mode (TE_{1m})

Figure 3.5: Double corner-cut cavity e-field

4

Design

4.1 Method

The project will follow a general engineering design process. An iterative process with short deadlines ensures that less time is spent on solutions that won't hold up to the stated specifications. The design steps are as follows:

1. Identify possible solutions how to achieve the specified polarization that can work interchangeably with an orthogonal polarization an using identical feeding network.

2. Implement the design and calculate far field patterns, scattering parameters, directivity and radiation efficiency in CST Microwave. If the simulation results prove it to be necessary, go back to the first step and evaluate new solutions to tackle the problem.

3. Manufacture a prototype of the antenna and compare the simulated parameters with the real world result.

4. Present, compare and discuss one or multiple designs which conform to the specification.

4.2 Antenna specifications

5G mobile telephone systems will use above 6 GHz bands to provide the high broadband speeds envisioned by the standard makers. The 28 GHz band has been licensed by telecommunication regulation agencies world wide to provide around 2 GHz of bandwidth for the next generation system. However, different interests by different organizations has made global harmonization problematic and the licensed test spectra are slightly different world wide, going as low as 24.5 GHz in Europe, up to 29.5 GHz in South Korea and Japan[25].

The stated objective is to cover as large portion as possible over the frequency range of 27 GHz to 31 GHz, which is the bandwidth of the already designed corresponding longitudinal slot array antenna. The antenna should at least achieve the following specifications.

- 8 x 8 ridge gap wave guide slot array antenna
- Frequency range: 27 GHz to 31 GHz
- Beam steering: $\pm 45°$ degrees on the azimuth axis, slight steering in elevation
- Side lobe level: -13.3 dB
- Cross polarization: -30 dB
- Input reflection coefficient: -10 dB
- Total efficiency: -0.5 dB
- Gain: 24 dB

From a manufacturing perspective, the solution should not add more than a few millimeters in additional thickness compared to the standard slot antenna. It should also not add too many extra layers as the space is too limited to add any gap wave guide pin structure to cancel any wave propagation between the layers.

4.3 Double cut cavity unit cell

The use of the corner cut cavity allows for a very compact solution, adding less than $\lambda/4$ in thickness compared to the normal longitudinal slot antenna. The structure is simulated as a generalized unit cell to design and evaluate the performance. As the slots are placed with alternating offset of the excitation elements from the center of the waveguide, the unit cell is simulated over twice the individual element period. The structure is designed in three layers, the gap ridge waveguide feeding layer, the excitation and twist layer, and the radiation layer. The unit cell boundaries were drawn in the middle of the row of pins along the waveguide and directly between two slots along the waveguide.

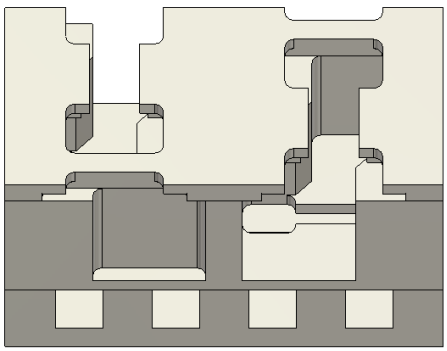

Figure 4.1: Double cut cavity unit cell

4.3.1 Feeding layer

The bottom layer is a ridge gap waveguide responsible of feeding the energy to the individual elements in the sub array. The waveguide walls are comprised of a single row of pins to isolate the energy from the adjacent waveguides.

Pin height	Pin width	Pin period	Band gap
2.1 mm	1.35 mm	2.65 mm	23.75 GHz - 56.5 GHz

Table 4.1: Pin dimensions

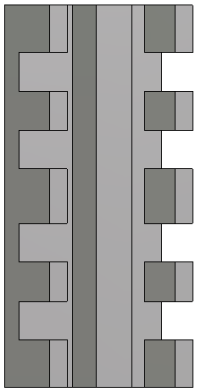

Figure 4.2: Feeding layer geometry.

The feeding waveguide is designed around the element spacing requirements set by the beam steering. The width of the waveguide is limited by the maximum width for azimuth scanning. At 31 GHz this can be calculated with Eq. 3.7 to 5.67 mm. Taking width of the gap waveguide pins into account gives us a maximum width of 4.32 mm. The element spacing in the elevation direction is decided by the guided wavelength as the slots are to be placed $\lambda_g/2$ apart for uniform excitation. The element spacing is chosen to 6.5 mm.

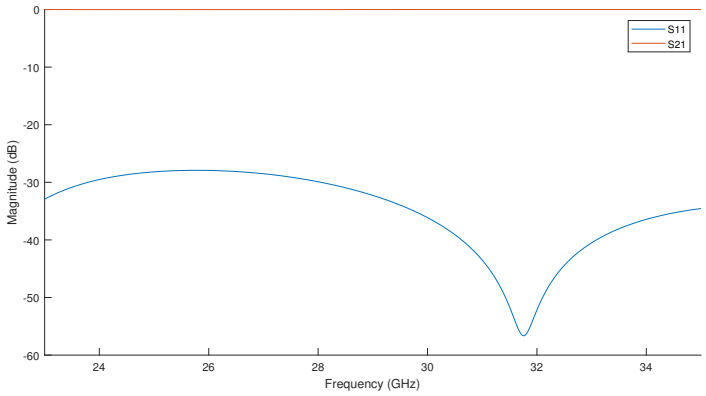

Figure 4.3: Ridge gap waveguide S-parameters without slots.

Width	Height	Ridge width	Ridge height	λ_g at 29 GHz
4.25 mm	2.1 mm	1.4 mm	1.6 mm	13 mm

Table 4.2: Feeding layer ridge waveguide dimensions

4.3.2 Cavity layer

The cavity layer is comprised of a slot with a ridge inset exciting a corner cut cavity placed on top. The cavity supports a field distribution with a dominant mode oriented at a 45 degree angle across the ridge as well as a secondary mode orthogonal to the dominant which results in an elliptically polarized electric field inside the cavity.

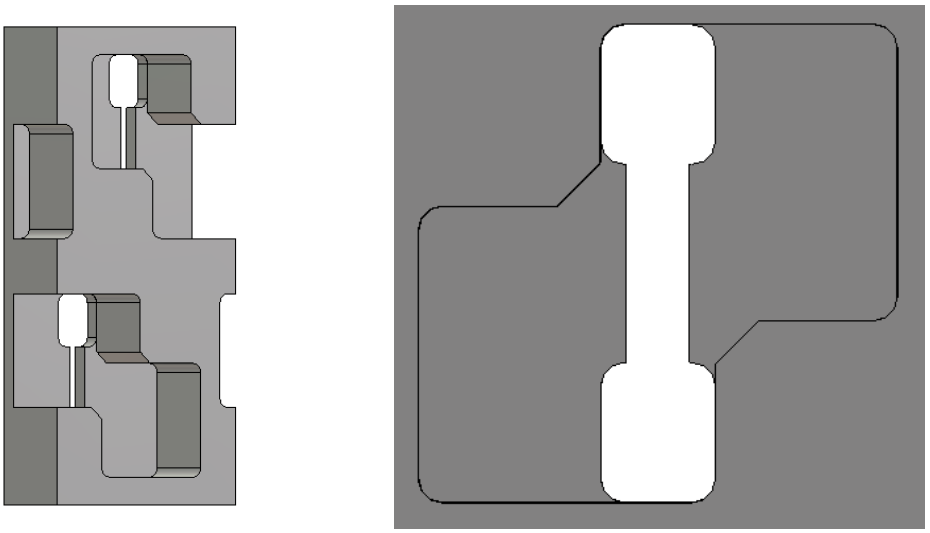

(a) Cavity layer **(b)** Cavity layer outline

Figure 4.4: Cavity layer geometry

The structure has a couple of frequency dependent parameters. The first is the position of the excitation slots along the waveguide. For optimal excitation, the slots need to be placed $\lambda_g/2$ apart on alternating sides of the waveguide to keep the excitation in phase. The next parameter is the shape and size of the excitation slot. The cavity limits the slot to a maximum length of 5 mm, which is shorter than required for the slot to resonate at 29 GHz. To mitigate this, the bandwidth of the slot is increased by introducing a ridge for a dumbbell-like shape.

Slot height	Slot width	Slot ridge height	Slot ridge width
1.2 mm	5.0 mm	0.37 mm	2.09 mm

Table 4.3: Excitation slot dimensions

Cavity depth	Cavity width	Cavity corner cut inset
2.36 mm	5.0 mm	1.9 mm

Table 4.4: Corner cut cavity dimensions

4.3.3 Radiation elements

The radiation slots are oriented orthogonal to the excitation slots and are excited by the e-field component inside the cavity that is longitudinal to the waveguide propagation. Because the main scanning axis is in the h-plane of the radiating slot, the width of the slot is highly constrained by the narrow element spacing which means that the usual $\lambda/2$ wide resonant slot is too large. Instead, the shorter width is compensated by making the slot higher, as well as introducing a double ridge to tune the impedance of the slot. The more square slot has the drawback that the polarization isolation is not as good.

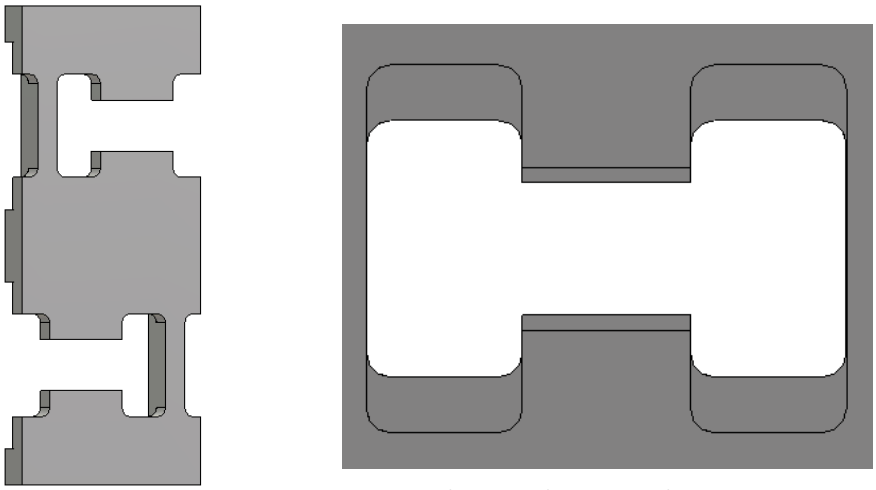

(a) Radiation layer

(b) Radiation layer outline

Figure 4.5: Radiation layer geometry

The transition from the corner cut cavity to the radiation slot is stepped in order to attenuate the unwanted polarization. The step leads to a more symmetrical distribution in the slot which increases the cross polarization isolation because the phase of the cross polarized e-field on the sides of the ridge are 180° out of phase.

Slot height	Slot width	Slot ridge height	Slot ridge width
4.54 mm	5.0 mm	1.24 mm	1.83 mm

Table 4.5: Inner radiation slot dimensions

Slot height	Slot width	Slot ridge height	Slot ridge width
2.79 mm	5.0 mm	0.70 mm	2.26 mm

Table 4.6: Outer radiation slot dimensions

4.3.4 Unit Cell Simulations

The unit cell is simulated in CST with unit cell boundary conditions assuming equal amplitude and phase excitation of all elements. As we can see in 4.6 the unit cell has a flat frequency response over the frequencies of interest. The bandwidth is limited by the wavelength dependent period of the elements. The radiated power is on the lower end, peaking at −3.8 dB for the co-polar floquet port with a cross-polar isolation of 18 dB.

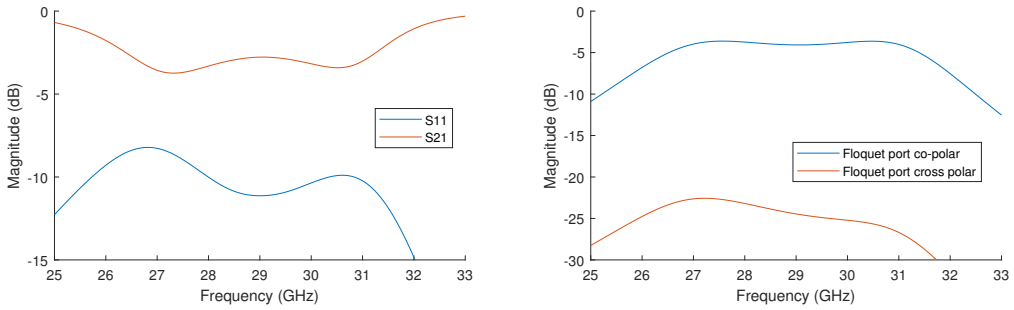

(a) Waveguide port S-parameters **(b)** Floquet port S-parameters

Figure 4.6: Unit Cell S-parameters

The phase and amplitude errors of the e-field at the center of the radiating slots are shown in Fig. 4.7. The amplitude error is explained by a lower excitation of the second slot due to the power lost from the radiation from slot 1. In this simulation, the slot offset from the waveguide center were kept the same. When feeding the slots from the real feeding waveguide, the offset can be used to fine tune the excitation amplitude. The phase error is induced by the frequency dependent spacing between the individual slots. The slot spacing for the unit cell was 6.5 mm, corresponding to $\lambda_g/2$ for the feeding

waveguide at 29 GHz, which corresponds to the 0° crossing at 29 GHz.

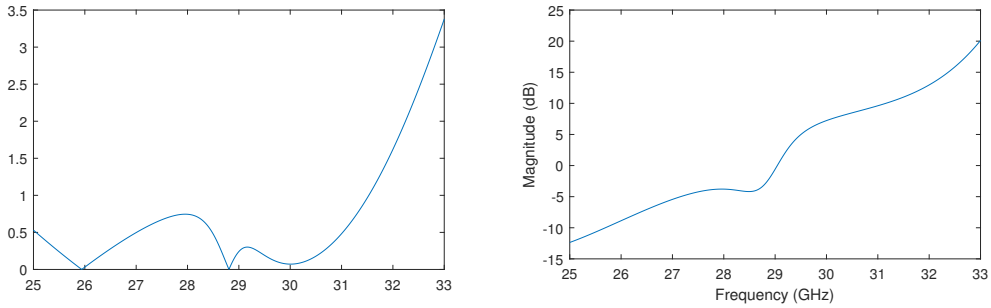

(a) Unit cell slot amplitude difference **(b)** Unit cell phase difference

Figure 4.7: Unit cell slot amplitude and phase difference

The radiation pattern of the unit cell is slightly frequency dependent due to the changing electrical length between the two cavities. The gain is highest at the design frequency of 29 GHz and drops about 1 dB at the edges of the frequency range. Also of interest is the gain drop in the H-plane which in our case is the plane were most of the scanning is performed. At ±40°, the gain starts to drop quickly, however this (together with the sidelobes) is most likely an artifact from reflections in the simulated infinite ground plane. However, a few dB of gain reduction will be seen for higher scanning angles in azimuth due to the inherent lack of rotational symmetry for the slot farfield pattern in the H-plane.

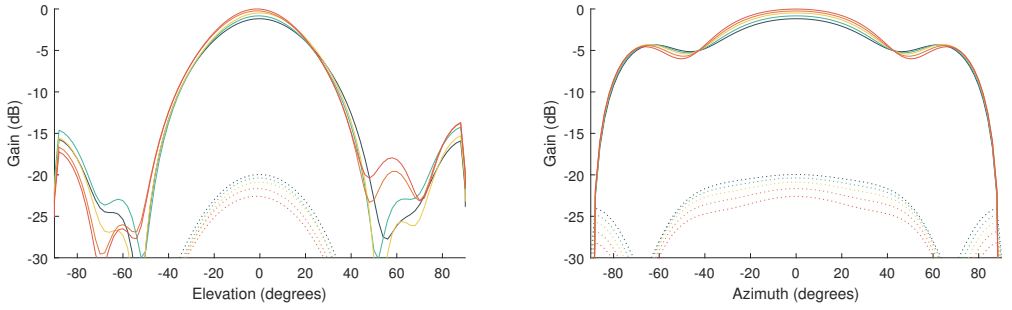

(a) E-plane. $G_{max} = 9.65\,\text{dB}$ **(b)** H-plane. $G_{max} = 9.65\,\text{dB}$

Figure 4.8: Unit cell farfield

4.3.5 Unit Cell E-field

The E-field in the structure gradually transforms between horizontal and vertical polarization. As we can see in Fig. 4.9 the coupling is mainly between the transverse component of the slot E-field. Thus, the minimum height of the structure is limited by the distance it takes for the e-field to transform from the radial distribution around each slot to the transverse fundamental mode of the double-corner-cut square waveguide.

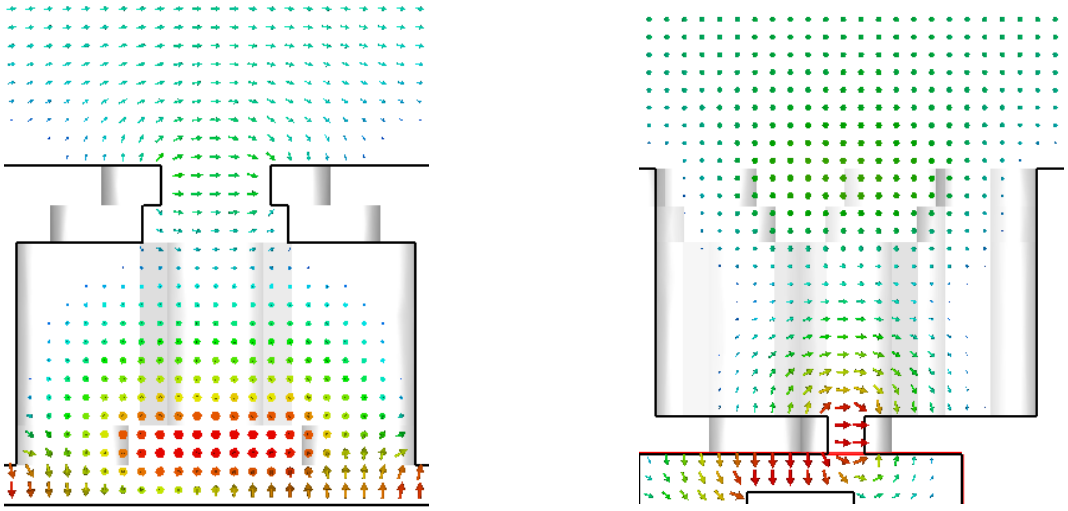

(a) Radiation slot E-plane cut

(b) Radiation slot H-plane cut

Figure 4.9: Simultaneous cross section of e-field.

4.4 Feeding layer

The feeding layer is responsible for distributing the energy from the waveguide port to the slots. Each column of the array is fed by a pair of ridge waveguides seen in Fig. 4.10.

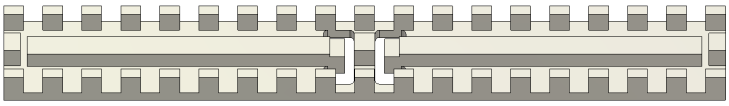

Figure 4.10: Periodic feeding layer

The waveguides are fed from the center of the unit cell and terminated by a short circuit at the edge of the array. The incoming and reflected wave creates a standing wave pattern along the ridge which is used to excite the individual array elements in series. The length of the waveguide is chosen to be approximately equal to two times the guided wavelength in order to fit four anti-nodes with amplitude maxima.

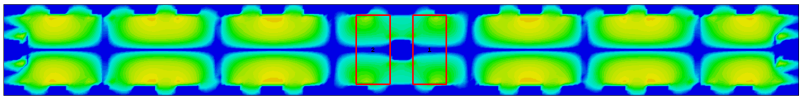

(a) Surface current at 27.5 GHz

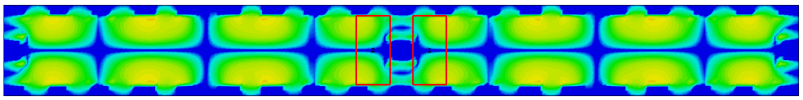

(b) Surface current at 28.5 GHz

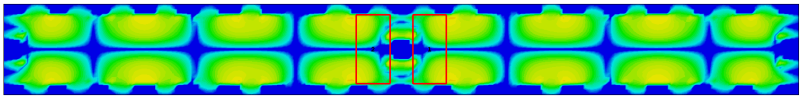

(c) Surface current at 29.5 GHz

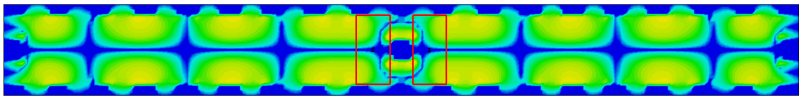

(d) Surface current at 29.5 GHz

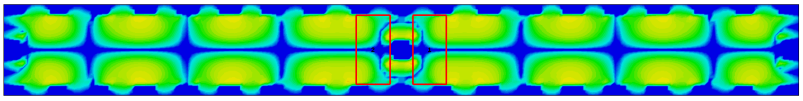

(e) Surface current at 30.5 GHz

Figure 4.11: Feeding layer top plate transverse surface current magnitude

4.4.1 Ridge waveguide bend

The input port of each sub-array is placed on the back of the antenna to provide easy access for passive elements such as filters as well as to the signal generating electronics. The port is connected to the distributing waveguide with a 90 degree waveguide E-bend.

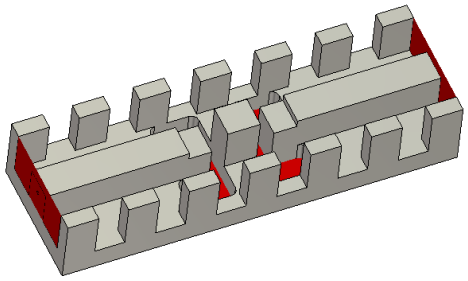

Figure 4.12: Feeding layer bend and isolation

The two feeding waveguides are isolated from each other with a gap waveguide pin in order to keep the standing wave patterns clean and without interference. Simulations show that the pin is successful in isolating the waveguides to 50 dB in the the studied frequency range. The simulated s-parameters for the slot-less feeding layer can be seen in Fig. 4.13. The scattering parameters are presented in reference to port 1, but can by s-parameter symmetry also be applied to the other ports.

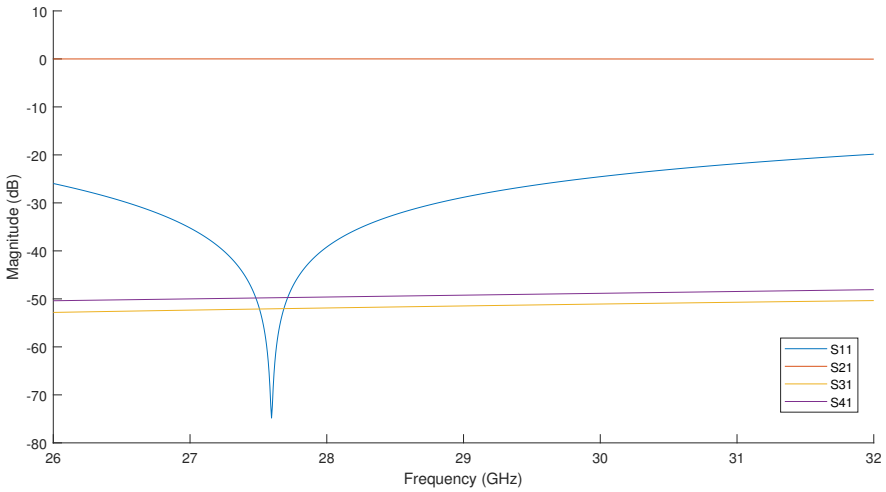

Figure 4.13: Feeding layer cross-talk

4.5 Double cut cavity array

The feeding layer is used to excite 8 elements in a linear array configuration, with 4 on the top and 4 on the bottom waveguide as seen in Fig. 4.14. The main goal is to achieve uniform amplitude and phase excitation of the slots as well as a low enough reflection coefficient to ensure that it is kept under $-10\,\mathrm{dB}$ while scanning.

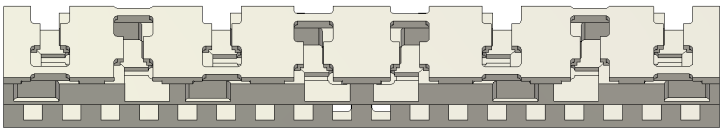

Figure 4.14: Linear array

Unfortunately, the design of the feeding layer presents a number of issues preventing us to achieve our goals. The feeding environment corresponds well with the unit cell for the second and third slot counting from the center outwards. But the first and outermost slots proved to be difficult to excite in uniform amplitude and phase with the rest. The outermost slot is located $\lambda_g/4$ from the short circuited end of the feeding waveguide, this interferes with the excitation of the slot but is deemed to be off less importance due to the positive effect tapering has on the side lobe levels. More urgent is the difficulties to excite the slot closest to the feeding waveguide as a low excitation amplitude has a large impact on the side lobe levels.

4.5.0.1 Planar array configuration

The planar array is completed by placing 8 of the linear arrays side by side creating a 8 by 8 array with a total of 64 radiating elements grouped into 16 sub-arrays to provide interfaces for individual excitation for beam steering. Each waveguide port is conveniently placed in the center of the waveguide for easy access to additional layers or transitions to microstrip PCB.

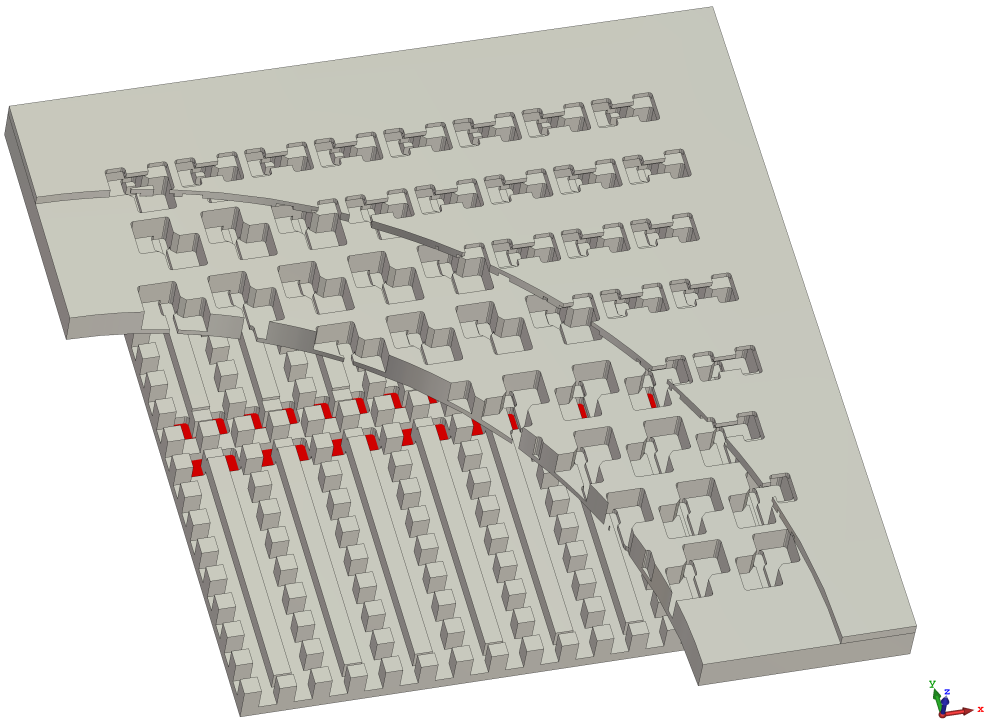

Figure 4.15: Array configuration

4.5.1 Full band design

The first design is over the entire frequency range of 27 GHz to 31 GHz. The design show that the unit cell simulations adequately provide a solution with sufficient bandwidth, however some issues regarding the feeding layer prevent the solution from fulfilling every specification.

4.5.1.1 Linear array S-parameters

The reflection coefficients for the individually excited ports are under −15 dB between 26 GHz and 31 GHz with a mutual coupling of less than −20 dB as seen in Fig 4.16a with no difference between the top and bottom waveguides. Exciting the ports simultaneously for broadside or for a 3 degree elevation scan angle has minimal effect on the impedance bandwidth as seen in 4.16b.

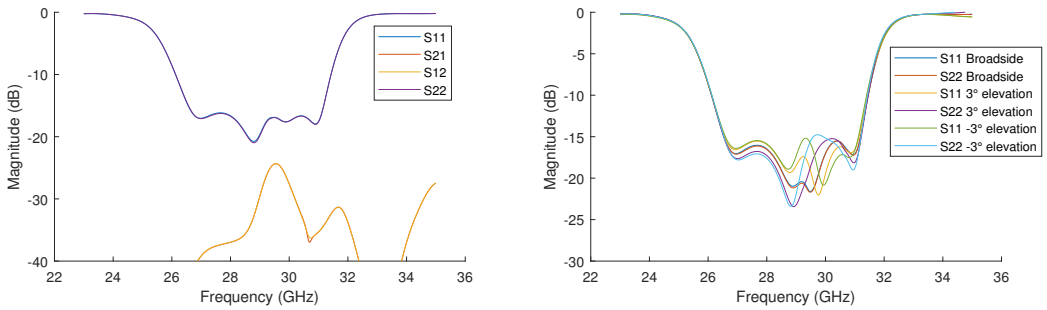

(a) Individual excitation **(b)** Simultaneous excitation

Figure 4.16: Periodic cell S-parameters

4.5.1.2 Linear array slot e-field phase and magnitude

The the farfield radiation pattern is highly dependent on the alignment of the excitation of the radiating slots in magnitude and phase. As a proof of concept, the goal of the array is uniform phase and amplitude excitation. Unfortunately, the first slot closest to the center of the array is not sufficiently excited and suffers from a phase and amplitude offset from the rest of the slots as seen in Fig. 4.17 and 4.18. The maximum magnitude error is 5.8 dB at 27 GHz

and the maximum phase error is 50° at 27.7 GHz. Otherwise, the slots show a rather flat frequency response over the range of interest. Which suggests that the limitation comes from the excitation between the feeding waveguide and the twist.

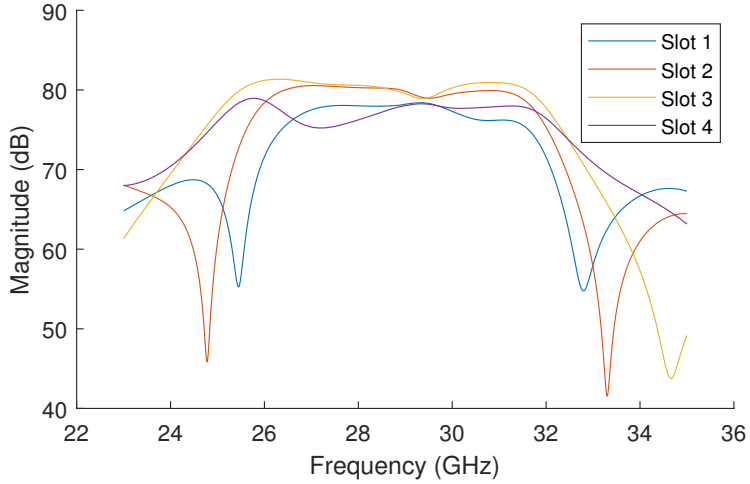

Figure 4.17: Slot E-field Magnitude

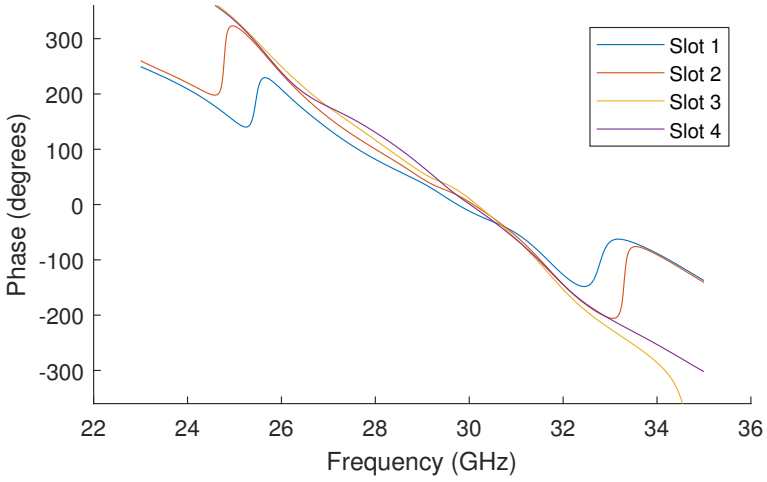

Figure 4.18: Slot E-field Phase

4.5.1.3 Linear array farfield

The higher phase error for lower frequencies shows itself in the radiation pattern, seen in Fig. 4.19, with higher sidelobes and lower directivity as a result. Above 27 GHz, the sidelobes are under −10 dB.

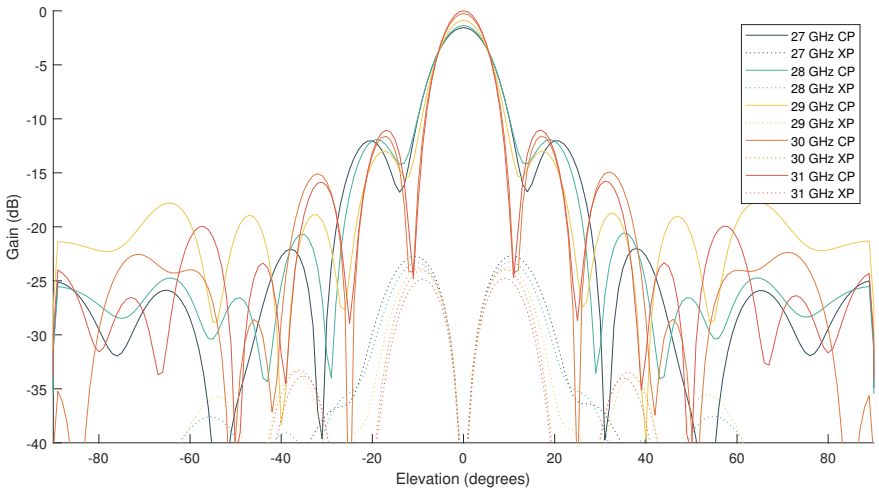

Figure 4.19: Periodic cell e-plane farfield with no scanning. $G_{max} = 15.4\,\text{dB}$

Under 28 GHz we get an increased first sidelobe, with a maximum of −11 dB at 27.5 GHz. Above 28 GHz, the amplitude distribution is tapered towards the edge of the array, reducing the sidelobes down to −13 dB at 29.5 GHz.

The gain is stable over the frequency range, going from 14.4 dB at 27.5 GHz to 14.8 dB at 29.5 GHz, with a minimum cross polarization isolation at 21 dB at 27.5 GHz.

As the periodic cell column consists of two sub arrays, it is possible to steer the beam slightly in elevation. The scanning is limited by the slot grouping in elevation because we can only control the phase of the two sub arrays and not the slots individually. A scanning angle of just 3° quickly reduces the performance with side lobes well over −10 dB at scanning angles as low as -3 degrees. Scanning further up or down increases the side lobe levels drastically with lower gain as a result. When the phase shift between the top and bottom sub array is 180^{circ}, the main beam is fully split. Interesting to note is that

when the co-polar radiation goes from even to odd symmetry, the cross-polar radiation does the opposite. This is because the antenna array is mirrored over the H-plane of the antenna, resulting in an inversion of the phase in the H-plane and not in the E-plane.

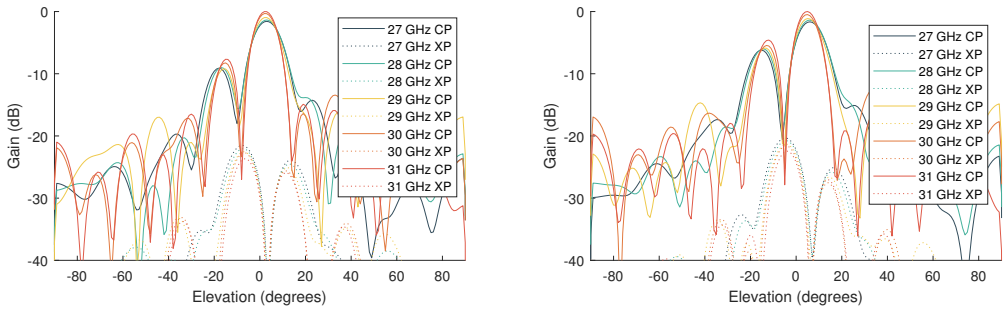

(a) 3 degree scanning $G_{max} = 15.3\,\mathrm{dB}$ **(b)** 5 degree scanning $G_{max} = 14.8\,\mathrm{dB}$

Figure 4.20: Periodic cell E-plane elevation scanning

4.5.1.4 Planar array S-parameters

While scanning ±45° in azimuth, the S-parameters for the 3 columns towards the steering are degraded above −10 dB due to mutual coupling.

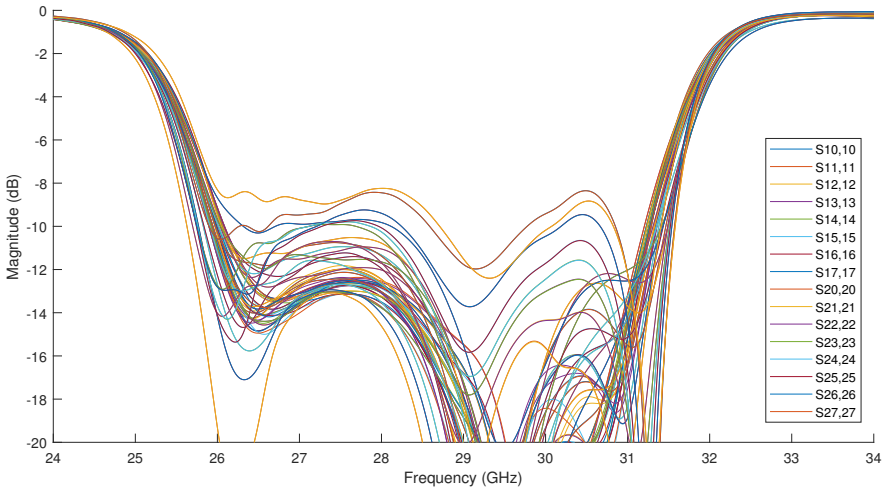

Figure 4.21: Array S-parameters ±0°, ±15°,±35°, and ±45° in azimuth

4.5.1.5 Planar array radiation pattern

In the azimuth plane (H-plane) the farfield pattern corresponds to the theoretical case with equal amplitude and no phase offset. Because the scanning is done in the H-plane there is a slight loss in gain when scanning compared to the broadside case. This is inherent due to the semi-toroidal shaped radiation pattern of the individual slots. The loss in directivity is around 2 dB for a scanning angle of 45° with slightly worse performance in the lower part of the bandwidth. The same reduction is not seen for the cross-polarized radiation, which means that the cross-polar isolation is also reduced for wider scanning angles.

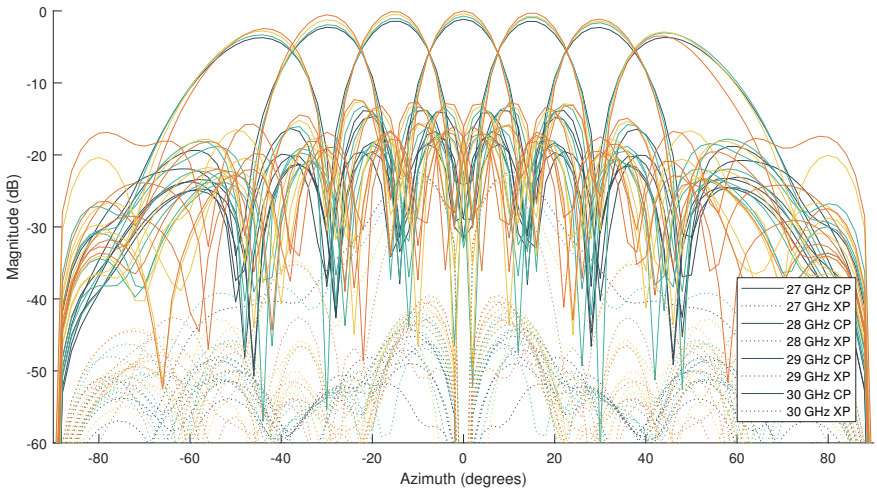

Figure 4.22: H-plane gain

4.5.2 Sub band design

The unit cell design proved to not be good enough together with the feeding layer to achieve the design goals over the entire frequency range of interest. Instead, it was decided to optimize the linear array for a narrower frequency band of of 27.5 GHz to 29.5 GHz, corresponding to the bandwidth of a single 5G test band.

4.5.2.1 Linear array S-parameters

The reflection coefficients for the individually excited ports are under −10 dB between 27.5 GHz and 29.5 GHz with a mutual coupling of less than −30 dB. Exciting the ports simultaneously for broadside or for a 3 degree scan angle has minimal effect on the reflected power.

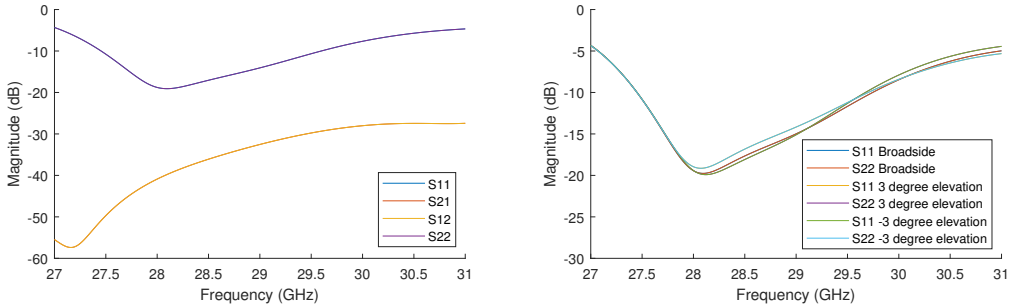

(a) Individual excitation **(b)** Simultaneous excitation

Figure 4.23: Periodic cell S-parameters

4.5.2.2 Linear array slot e-field phase and magnitude

The the farfield radiation pattern is highly dependent on the alignment of the excitation of the radiating slots in magnitude and phase.

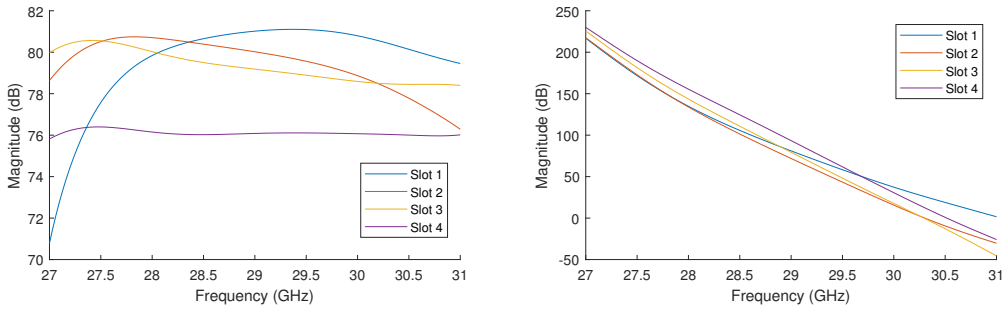

(a) Slot E-field Magnitude **(b)** Slot E-field Phase

Figure 4.24: Slot phase

4.5.2.3 Linear array farfield

The frequency dependent excitation of the first slot influences the sidelobe levels. Under 28 GHz we get an increased first sidelobe, with a maximum of −11 dB at 27.5 GHz. Above 28 GHz, the amplitude distribution is tapered towards the edge of the array, reducing the sidelobes down to −13 dB at 29.5 GHz.

The gain is stable over the frequency range, going from 14.4 dB at 27.5 GHz to 14.8 dB at 29.5 GHz, with a minimum cross polarization isolation at 21 21 dB at 27.5 GHz.

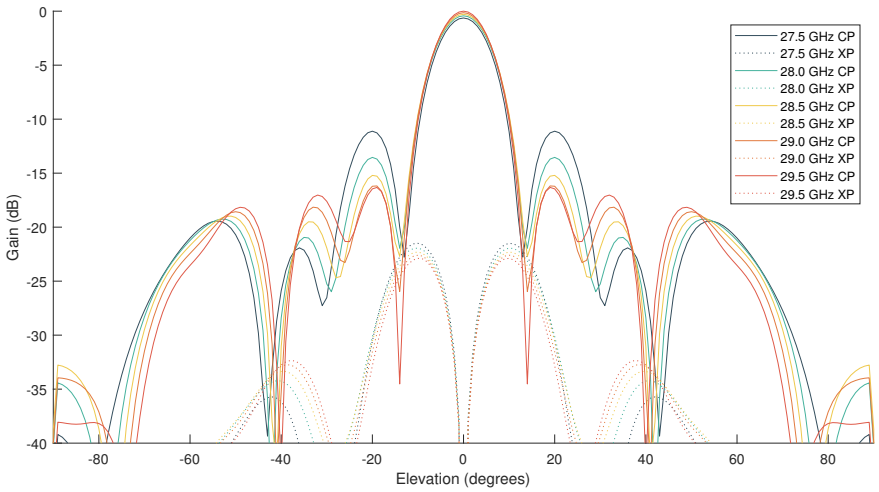

Figure 4.25: Periodic cell e-plane farfield with no scanning. $G_{max} = 14.8\,\text{dB}$

The sub band design shares the problem with elevation scanning with the full band design. A scanning angle of just 3° quickly reduces the performance with side lobes well over −10 dB at scanning angles as low as -3 degrees.

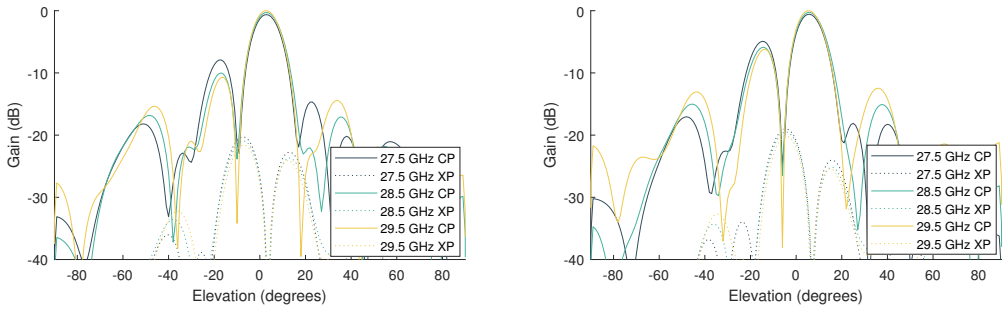

(a) 3 degree scanning. $G_{max} = 14.6\,\text{dB}$ **(b)** 5 degree scanning. $G_{max} = 14.1\,\text{dB}$

Figure 4.26: Periodic cell E-plane elevation scanning

4.5.2.4 Planar array S-parameters

The reflection coefficients for the individually excited sub arrays, shown in Fig. 4.27a, are less than −10 dB from 27.2 GHz to 29.6 GHz and less than −20 dB from 27.5 GHz to 29.0 GHz. The cross coupling, shown in Fig. 4.27b, is at most −20 dB between two adjacent columns and −25 dB between two adjacent rows.

For simultaneous excitation, shown in Fig. 4.28, the reflection coefficient is less than −10 dB from 27.5 GHz to 29.5 GHz for azimuthal scanning from −45° to 45° and elevation scanning from −5° to 5°. Beam scanning has a large impact on the reflection coefficient due to cross-coupling between the slots, degrading the reflection coefficient with almost 10 dB.

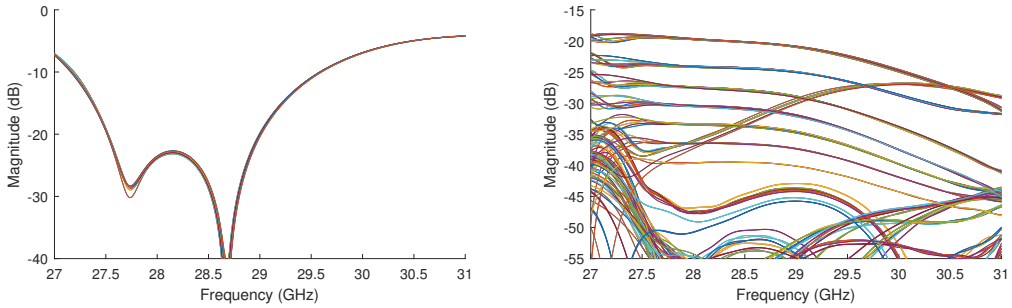

(a) Individual excitation s-parameters **(b)** Sub array cross coupling

Figure 4.27: Array S-parameters individual excitation

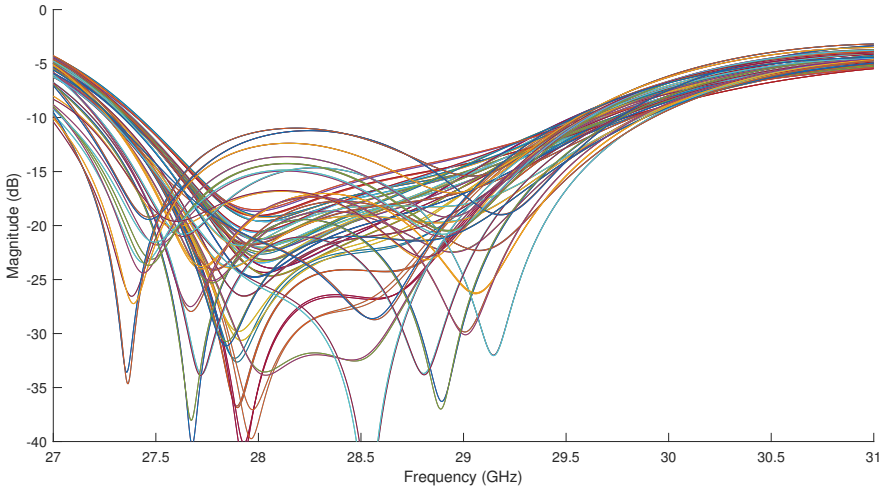

Figure 4.28: Array S-parameters +-0, +-15, +-30, +-45 in azimuth as well as +-3,5 degrees in elevation

4.5.2.5 Planar array radiation pattern

The E-plane for broadside scan shown in Fig. 4.30 has not changed significantly from the periodic simulations and retains the performance issues to to the non-uniform phase and amplitude excitation of the slots. In Fig. 4.31, the antenna gain and cross-polar isolation is shown over frequency and azimuth scanning, where we clearly can see the reduced performance for the lower part of the frequency range.

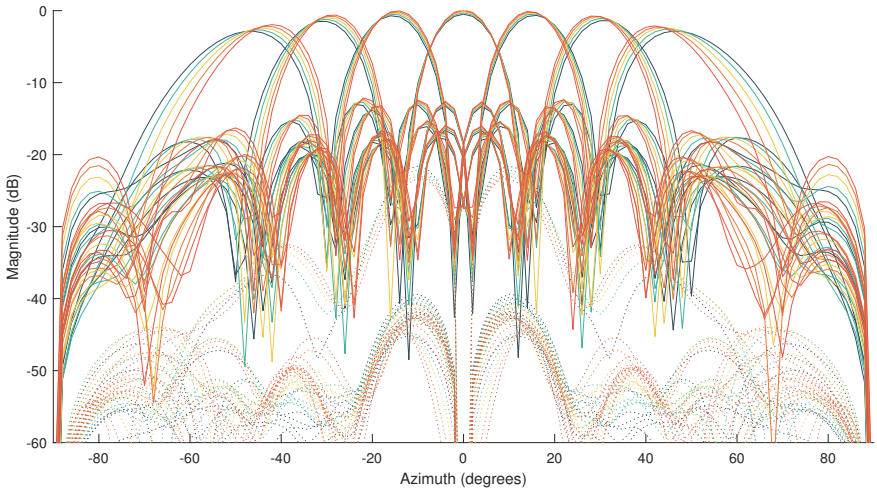

Figure 4.29: H-plane gain. $G_{max} = 23.9\,\mathrm{dB}$

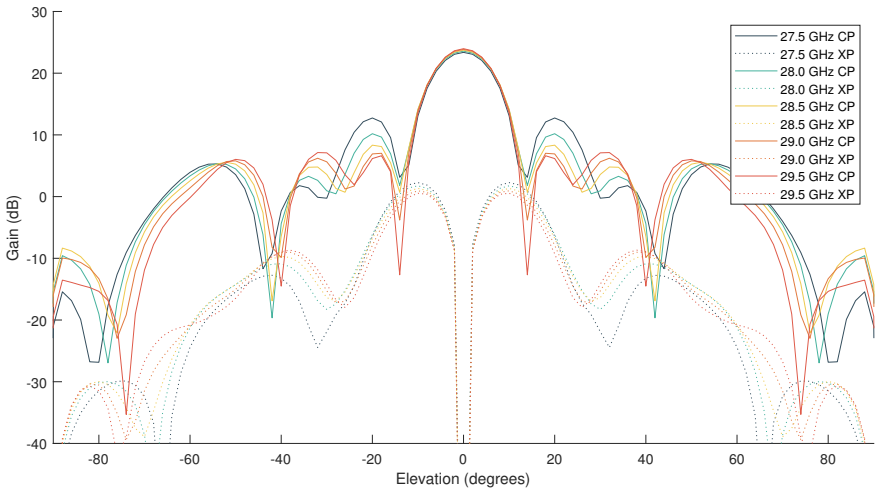

Figure 4.30: Array e-plane farfield with no scanning.

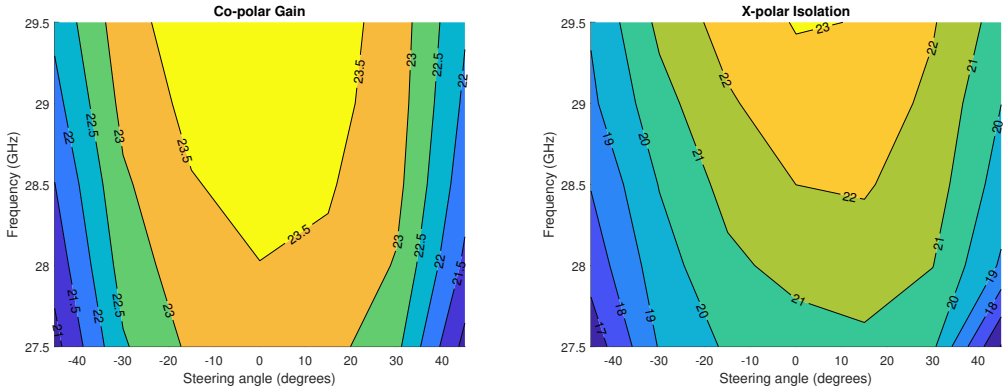

(a) Co-polar Gain **(b)** Cross polar isolation

Figure 4.31: Array S-parameters individual excitation

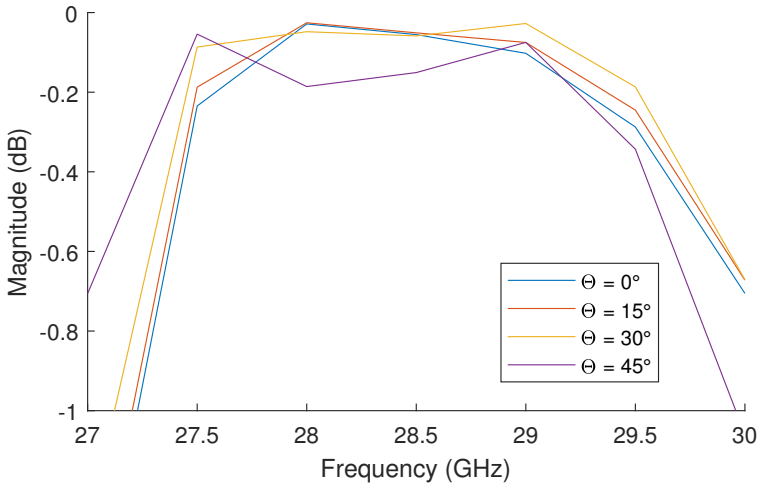

Figure 4.32: Planar array total efficiency for different steering angle Θ

4.5.2.6 Sensitivity analysis

The antenna is designed in three layers to allow for production by routing. For the antenna to work as designed, it is important that no wave propagation or leakage in an eventual gap between the layers which might occur due to imprecise production. For the gap between the feeding layer and the cavity layer, any propagation is stopped with the pin based AMC and thus presents no issue due to the gap waveguide technology. Unfortunately, the design of the cavity layer did not allow for the use of the AMC for the gap between the cavity layer and the radiation layer due to limited space. This leads to a probable issue for manufacturing. Simulations were made with a 0.05 mm gap between the cavity and radiation layer, which can be seen in Fig. 4.33. The degraded reflection coefficient reduces the bandwidth for the broadside excitation with 0.5 GHz and leaves no margin for scanning.

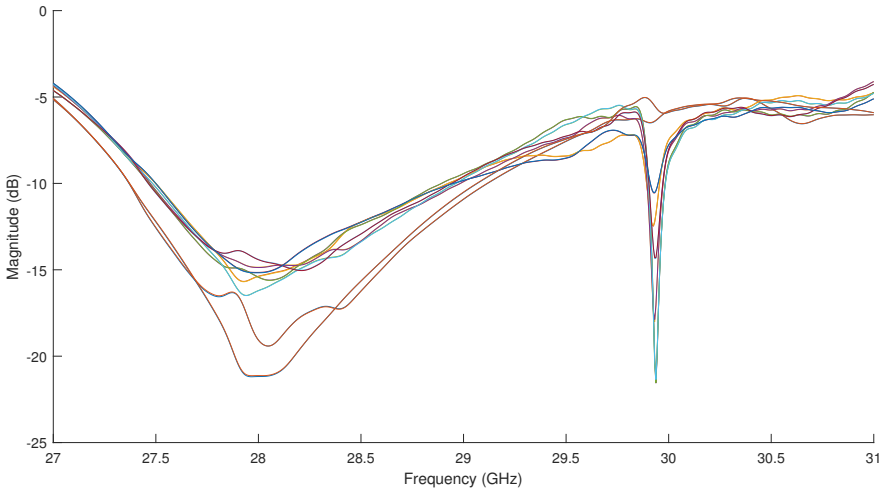

Figure 4.33: S-parameters for 0.05 mm gap broadside excitation.

5

Results

A prototype (seen in Fig 5.1, 5.2 and 5.3) was milled in aluminum based on the sub band design and assembled with the test rig outfitted with waveguide to coaxial cable transitions as an interface.

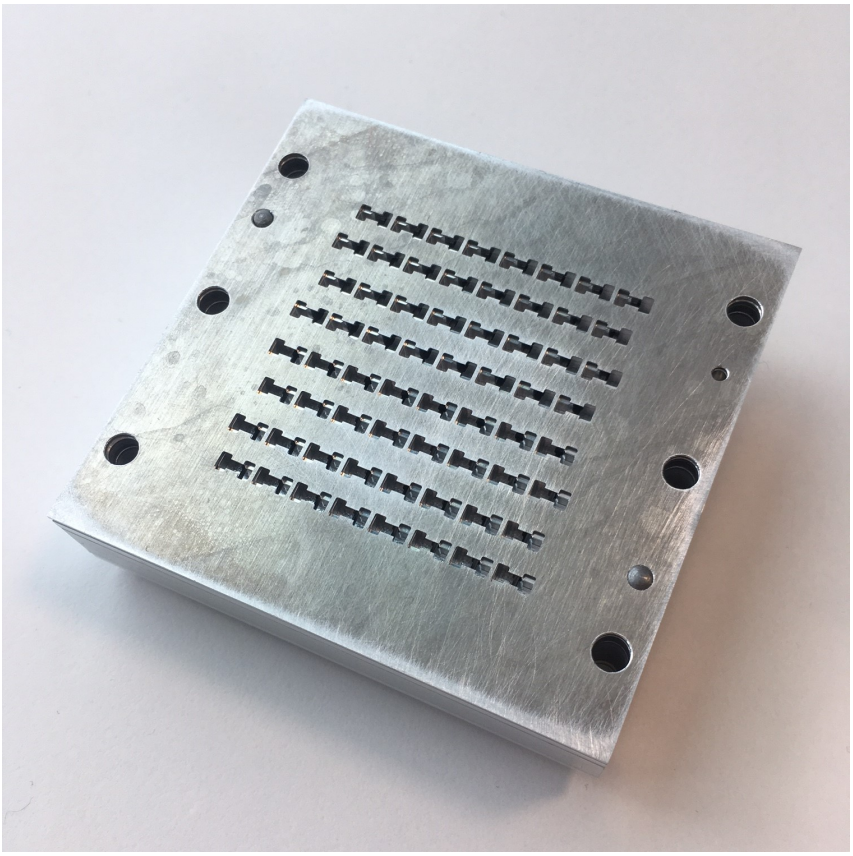

Figure 5.1: Assembled prototype

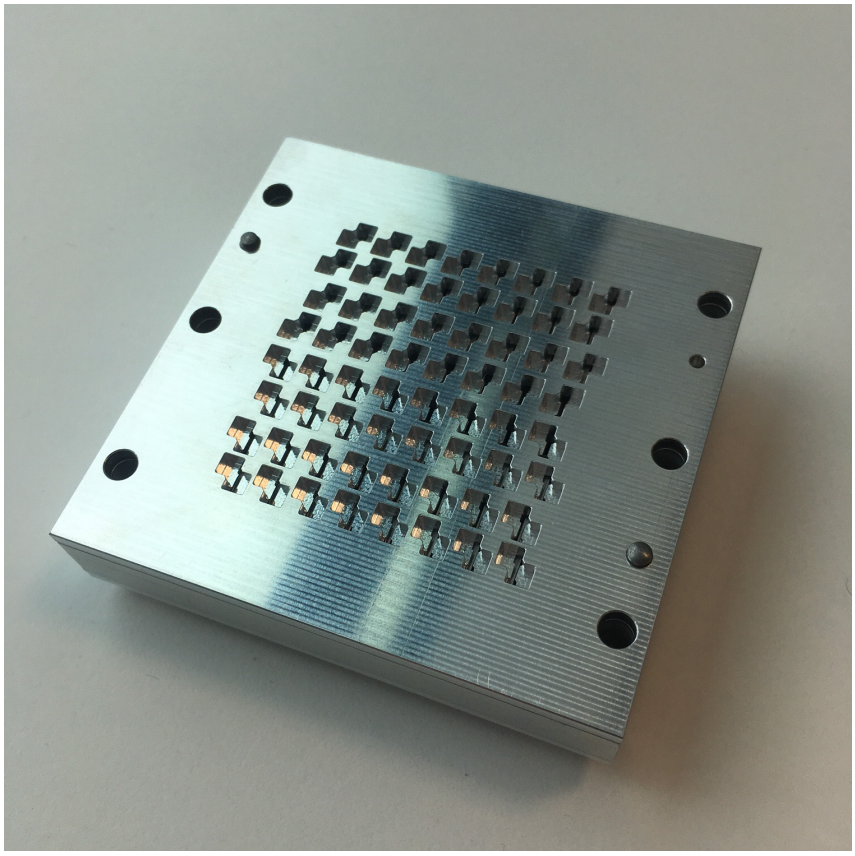

Figure 5.2: Prototype cavity layer

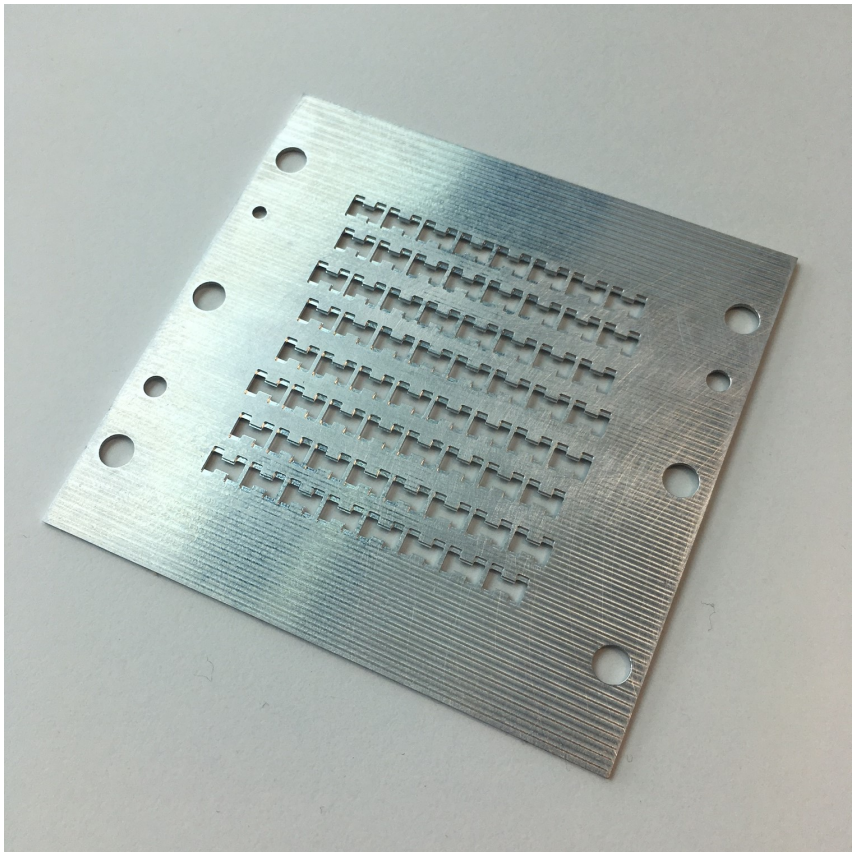

Figure 5.3: Prototype bottom of cavity layer

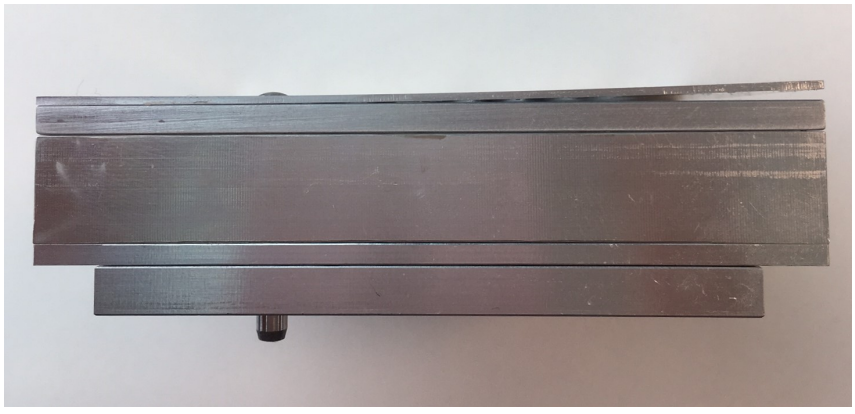

Figure 5.4: Prototype radiation layer flex

Unfortunately, the radiation was delivered slightly crooked, which can be seen in 5.4. Most of the gap can be closed with the tightening pins, but as the simulations show, a small gap between the cavity and excitation layer has a big impact on the reflected power.

After assembly, the antenna performance was tested for impedance matching and farfield radiation pattern.

5.1 S-parameters

The impedance matching of each sub-array as well as the isolation between was measured with a vector network analyzer. The results can be seen in Fig. 5.5 and 5.6.

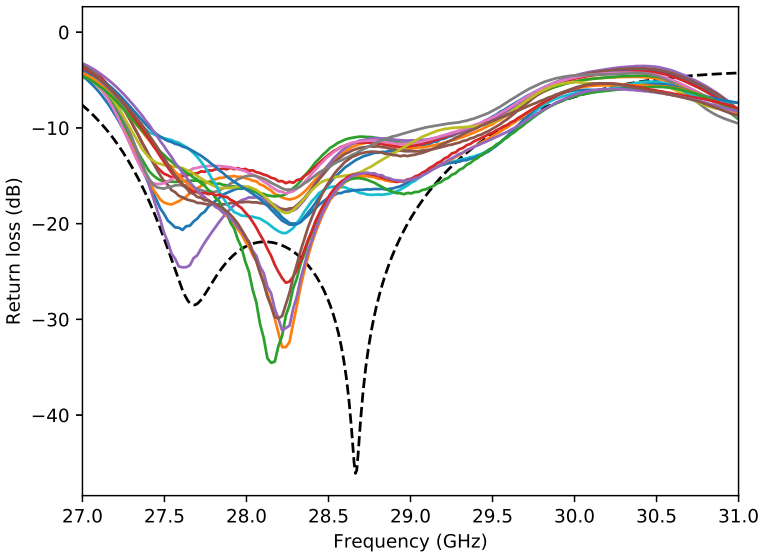

Figure 5.5: Measured return loss, compared with simulation (dashed)

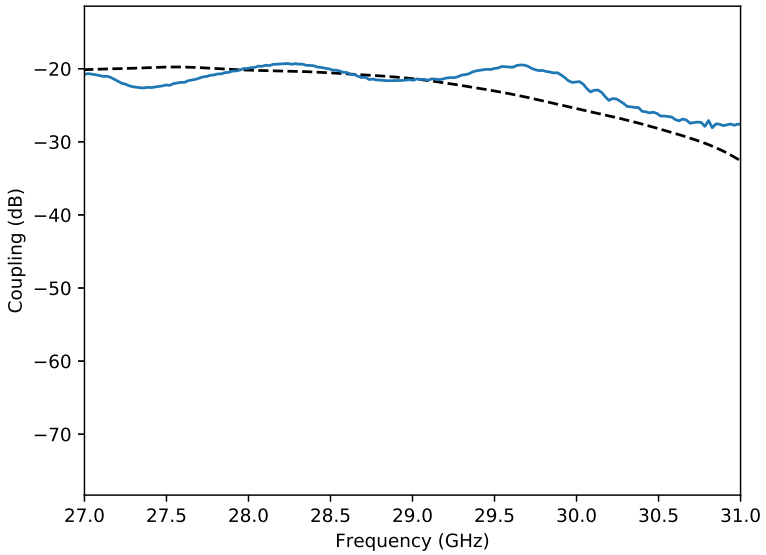

Figure 5.6: Measured coupling between two adjacent columns, compared with simulation (dashed)

5.2 Farfield pattern and gain

After the verification of the impedance performance, the antenna was tested in an anechoic chamber to measure the farfield radiation pattern. The signal level of the measured peak is compared with a standard gain horn with 24 dB of gain in order to calculate the gain of the manufactured prototype.

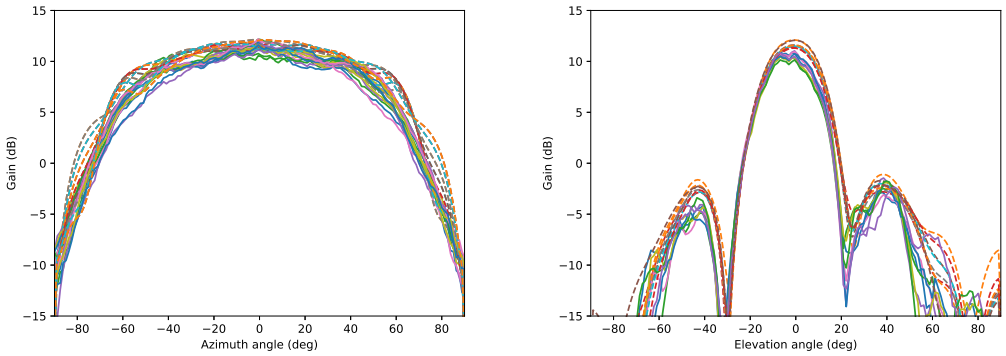

(a) Azimuth pattern **(b)** Elevation pattern

Figure 5.7: Farfield pattern for azimuth and elevation for all columns

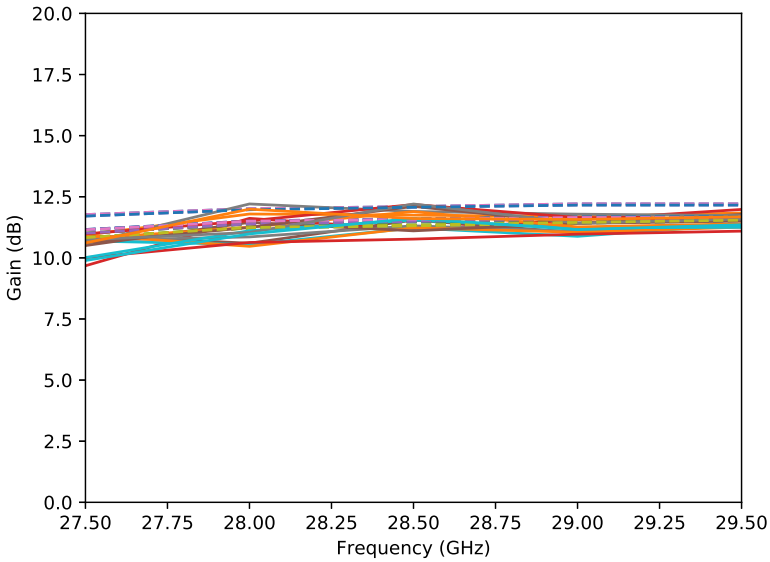

Figure 5.8: Measured gain over frequency, compared with simulation (dashed)

6

Conclusion

Some issues are identified where additional work is needed in order to improve the far field patterns as well as to increase the bandwidth of the antenna.

The bandwidth is limited by the excitation of the cavity from the feeding network. As we see in the unit cell simulations in 4.6, the cavity has a flat frequency response over the frequency range of interest. The problem with achieving the antenna specifications occur when we go from the infinite rectangular waveguide of the unit cell to the terminated resonant waveguide in the linear array.

In the linear array, the slot spacing is reduced to 6.2 mm from 6.5 mm in order to keep compatibility with the already existing design. This leads to slightly higher phase error, which results in higher sidelobes and lower directivity. The two slots that are most affected by the change in topology is the slot closest to the center (slot 1) and the slot closest to the termination (slot 4). The input reflection coefficient of the linear array is highly dependent on the excitation of slot 1. The cavity presents a rather large reflection coefficient towards the source which is highly correlated with the excitation of the slot, probably due to that the most of the reflection happens at the radiating slot. This imposes a constraint on the design which limits the ability to move the first slot to match the amplitude and phase with the rest of the slots.

6.1 Cross polarization isolation

We get a relatively low cross-polarization isolation due to the square slot design of the radiating slots. The slots are designed this way to provide good coupling to the elliptical polarized e-field inside the cavity to ensure a low reflection coefficient. If the coupling could be improved by introducing a change in the structure, the radiating slot could be made narrower which would increase the cross-polar isolation. As the antenna is designed to be used in a multipath environment, the cross polarization isolation is of less importance than in for example a point-to-point link where the lack of cross polar isolation directly influences the polarization diversity of the system.

6.2 Prototype manufacturing and verification

The prototype shows good correlation between measurement and simulation for the farfield pattern and cross coupling. The impedance matching is not as good as the full wave simulations predicted but are deemed passable due to the fact that the PCB to waveguide transition was not included in the antenna simulation which will influence the impedance mismatch. Another source of degradation is, as discussed earlier in the thesis, the fact that there was no place to introduce the gap waveguide pin-structure around the cavities, this means that the performance is greatly dependent on the galvanic contact between the cavity- and slot-layer. The realized gain is slightly lower, which can be explained by higher than anticipated losses in the feeding of the antenna during measurement. All in all, the prototype can be seen as a verification of the idea of using this type of mode-stirring cavity to modularly rotate the polarization of a slotted waveguide antenna by just adding a comparatively thin extra layer. The measurement of impedance matching and farfield pattern closed the design-loop and gave new insight into problems to be addressed in a future version.

6.3 Conclusion and future work

The work presented in this thesis show that it is possible to design a complementary set of orthogonally polarized series-fed slot array antennas with the use of a compact double cut corner cavity waveguide twist. To improve the performance of the antenna more work is needed to investigate how to decrease the relationship between the excitation of a slot and its reflection coefficient by improving the coupling between the cavity and the radiating slot.

Lastly, I'd like to thank my supervisors Ashraf Uz-Zaman at Chalmers and Carlo Bencivenni at Gapwaves as well as my examiner Jian Yang at Chalmers

Bibliography

[1] E. Rajo-Iglesias, M. Ferrando-Rocher, and A. Zaman, "Gap waveguide technology for millimeter-wave antenna systems," *IEEE Communications Magazine*, vol. 56, pp. 14–20, 07 2018.

[2] A. U. Zaman and P.-S. Kildal, *GAP waveguides, Handbook of Antenna Technologies*, 2016, pp. 3273–3347.

[3] C. Bencivenni, T. Emanuelsson, and M. Gustafsson, "Gapwaves platform integrates 5g mmwave arrays," *Microwave Journal*, vol. 20, pp. 23–29, 09 2019.

[4] K. Kibaroglu, M. Sayginer, T. A. Phelps, and G. M. Rebeiz, "A 64-element 28-ghz phased-array transceiver with 52-dbm eirp and 8–12-gb/s 5g link at 300 meters without any calibration," *IEEE Transactions on Microwave Theory and Techniques*, vol. 66, pp. 5796–5811, 2018.

[5] P.-S. Kildal, *Foundations of antenna engineering.* Gothenburg, Sweden: Kildal Antenn, 2015.

[6] J. Helszajn, *Ridge Waveguides and Passive Microwave Components.* Reading, Massachusetts: Wiley, 2000.

[7] A. Haddadi, C. Bencivenni, and T. Emanuelsson, "Gap waveguide slot array antenna for automotive applications at e-band," *2019 13th European Conference on Antennas and Propagation (EuCAP)*, pp. 1–4, March 2019.

[8] A. Vosoogh, P. Kildal, and V. Vassilev, "Wideband and high-gain corporate-fed gap waveguide slot array antenna with etsi class ii radiation

pattern in v -band," *IEEE Transactions on Antennas and Propagation*, vol. 65, no. 4, pp. 1823–1831, April 2017.

[9] A. Vosoogh, A. Haddadi, A. Zaman, J. Yang, H. Zirath, and A. Kishk, "W-band low-profile monopulse slot array antenna based on gap waveguide corporate-feed network," *IEEE Transactions on Antennas and Propagation*, vol. PP, pp. 1–1, 10 2018.

[10] M. Ferrando-Rocher, J. I. Herranz-Herruzo, A. Valero-Nogueira, B. Bernardo-Clemente, A. U. Zaman, and J. Yang, "8 x 8 ka-band dual-polarized array antenna based on gap waveguide technology," *IEEE Transactions on Antennas and Propagation*, vol. 67, no. 7, pp. 4579–4588, July 2019.

[11] J. Liu, A. Vosoogh, A. Zaman, and J. Yang, "A slot array antenna with single-layered corporate-feed based on ridge gap waveguide in the 60-ghz band," *IEEE Transactions on Antennas and Propagation*, vol. PP, pp. 1–1, 12 2018.

[12] C. Bencivenni, M. Gustafsson, A. Haddadi, A. U. Zaman, and T. Emanuelsson, "5g mmwave beam steering antenna development and testing," *2019 13th European Conference on Antennas and Propagation (EuCAP)*, pp. 1–4, 2019.

[13] D. Zarifi, A. Farahbakhsh, and A. Zaman, "A gap waveguide-fed wideband patch antenna array for 60-ghz applications," *IEEE Transactions on Antennas and Propagation*, vol. PP, pp. 1–1, 07 2017.

[14] A. Zaman, T. Vukusic, M. Alexanderson, and P.-S. Kildal, "Design of a simple transition from microstrip to ridge gap waveguide suited for mmic and antenna integration," *Antennas and Wireless Propagation Letters, IEEE*, vol. 12, pp. 1558–1561, 12 2013.

[15] U. Nandi, A. Zaman, A. Vosoogh, and J. Yang, "Novel millimeter wave transition from microstrip line to groove gap waveguide for mmic packaging and antenna integration," *IEEE Microwave and Wireless Components Letters*, vol. PP, pp. 1–3, 07 2017.

[16] Y. Shi, J. Zhang, S. Zeng, and M. Zhou, "Novel w-band millimeter wave transition from microstrip line to groove gap waveguide for mmic integration and antenna application," *IEEE Transactions on Antennas and Propagation*, vol. PP, pp. 1–1, 03 2018.

[17] A. Zaman, V. Vassilev, H. Zirath, and N. Rorsman, "Novel low-loss millimeter-wave transition from waveguide-to-microstrip line suitable for mmic integration and packaging," *IEEE Microwave and Wireless Components Letters*, vol. 27, 11 2017.

[18] A. Aljarosha, A. Zaman, and R. Maaskant, "A wideband contactless and bondwire-free mmic to waveguide transition," *IEEE Microwave and Wireless Components Letters*, vol. PP, pp. 1–3, 04 2017.

[19] C. A. Balanis, *Antenna Theory*. Reading, Massachusetts: Wiley, 1993.

[20] L. Josefsson, "A waveguide transverse slot for array applications," *IEEE Transactions on Antennas and Propagation*, vol. 41, no. 7, pp. 845–850, July 1993.

[21] R. V. Gatti and R. Rossi, "A dual-polarization slotted waveguide array antenna with polarization-tracking capability and reduced sidelobe level," *IEEE Transactions on Antennas and Propagation*, vol. 64, pp. 1567–1572, 2016.

[22] D. Dogan and C. Top, "Circularly polarized ka-band waveguide slot array with low sidelobes," 03 2012.

[23] U. Rosenberg and R. Beyer, "Compact waveguide twist design fitting with interfacing waveguide cross sections," *2012 IEEE/MTT-S International Microwave Symposium Digest*, pp. 1–3, 2012.

[24] K. Anatoliy, D. Kulik, and L. Rud, "Compact 90 twist formed by a double-corner-cut square waveguide section," *Microwave Theory and Techniques, IEEE Transactions on*, vol. 56, pp. 1633 – 1637, 08 2008.

[25] J. Barrett. (2017) 5g spectrum bands. [Online]. Available: https://web.archive.org/web/20170830162655/https://gsacom.

com/5g-spectrum-bands/